Geochemistry, Geophysics, Geosystems®

RESEARCH ARTICLE
10.1029/2023GC011071

Geomorphology and Age Constraints of Seamounts in the Cabo Verde Archipelago, and Their Relationship to Island Ages and Geodynamic Evolution

Tom Kwasnitschka[1], Thor H. Hansteen[1], Ricardo S. Ramalho[2,3], Colin W. Devey[1], Andreas Klügel[4], Lisa K. Samrock[1], and Jo-Anne Wartho[1]

[1]GEOMAR Helmholtz Centre for Ocean Research Kiel, Kiel, Germany, [2]School of Earth and Environmental Sciences, Cardiff University, Cardiff, UK, [3]Departamento de Geologia, Faculdade de Ciências, Instituto Dom Luiz (IDL), Universidade de Lisboa, Lisboa, Portugal, [4]Fachbereich Geowissenschaften der Universität Bremen, Bremen, Germany

Abstract The Cabo Verde Archipelago is related to a mantle plume located close to the rotational pole of the African Plate. It consists of islands and seamounts arranged in a horseshoe-shaped pattern open to the west, thus forming two volcanic chains, each with a weak east-west age progression. High-resolution swath bathymetry of 12 Cabo Verde seamounts is used here to assign each seamount to its pre-shield, shield or post-shield evolutionary stage, respectively. The eastern seamounts exhibit degraded and partially eroded morphologies, and are mainly in their post-shield stage. A new ^{40}Ar-^{39}Ar date for Senghor Seamount at 14.872 ± 0.027 Ma supports old ages for the eastern seamounts. The western seamounts generally exhibit younger volcanic-edifice-construction morphologies, showing fresh effusive and explosive volcanics, including rarely observed deep-water explosive volcanism in the Charles Darwin Volcanic Field. Furthermore, the two previously unknown seamounts Sodade and Tavares in the westernmost termini of both volcanic chains exhibit pristine volcanic morphologies, in agreement with present-day volcanism and seismic activity recorded from the western seamounts. The islands and seamounts rest on three submarine platforms to the east, northwest and southwest, respectively. Taken together, the seamount and island data suggest a shift in igneous activity from the eastern to the other platforms at about 8–6 Ma. However, the complex evolution pattern for both volcanic chains includes the simultaneous occurrence of pre-shield or shield edifices at any time, followed by erosional and rejuvenation stages. The new seamount data still demonstrate ongoing westward submarine-growth in both volcanic chains.

Plain Language Summary The Cabo Verde volcanic islands and seamounts are located in the central Atlantic Ocean, ~570 km off the west coast of Africa. They form a horseshoe-shaped archipelago with two volcanic chains, which were formed by the African plate moving very slowly over a mantle hotspot (the Cabo Verde Plume). Both the northern and southern volcanic chains show weak east-to-west age progressions from ~26 million years to the present day. This study uses underwater topographic data and observations/rock sampling via remotely operated vehicles from 12 submarine volcanic seamounts, including two previously unknown seamounts, collected during four research cruises in the Cabo Verde Archipelago. Geomorphology is used to classify each seamount as being in its pre-shield, shield or post-shield evolutionary stage, respectively. Cabo Verde islands and seamounts rest on three submarine morphological platforms, reflecting westward jumps of the main igneous activity, and also confirming the westward migration of the Cabo Verde hotspot beneath both volcanic chains.

Key Points:

- We present bathymetrical maps of 12, in part previously uncharted Cabo Verde seamounts
- Geomorphology reflects various evolutionary seamount stages and relative ages. Four older seamounts indicate late Quaternary sea level lowstands
- Islands and seamounts rest on three morphological platforms, indicating westward jumps of the main igneous activity

Supporting Information:

Supporting Information may be found in the online version of this article.

Correspondence to:

T. Kwasnitschka,
tkwasnitschka@geomar.de

Citation:

Kwasnitschka, T., Hansteen, T. H., Ramalho, R. S., Devey, C. W., Klügel, A., Samrock, L. K., & Wartho, J.-A. (2024). Geomorphology and age constraints of seamounts in the Cabo Verde Archipelago, and their relationship to island ages and geodynamic evolution. *Geochemistry, Geophysics, Geosystems*, *25*, e2023GC011071. https://doi.org/10.1029/2023GC011071

Received 8 JUN 2023
Accepted 3 FEB 2024

Author Contributions:

Conceptualization: Thor H. Hansteen, Ricardo S. Ramalho, Jo-Anne Wartho
Data curation: Tom Kwasnitschka, Ricardo S. Ramalho, Colin W. Devey, Lisa K. Samrock, Jo-Anne Wartho
Formal analysis: Tom Kwasnitschka, Colin W. Devey, Andreas Klügel, Lisa K. Samrock, Jo-Anne Wartho

1. Introduction

The most obvious geomorphological expression of oceanic intraplate volcanism is seamounts and oceanic islands (Morgan, 1971). Subject to the relative motion and aging of the oceanic plate on which they are located, the life cycle of oceanic islands is governed by the interplay of volcanic activity, erosion, isostasy and plate flexure (Carracedo, 1999; Clague & Dalrymple, 1987; Johnson et al., 2018; Ramalho, 2011; Ramalho et al., 2010a, 2010b, 2013, 2017; Ramalho, Helffrich, et al., 2010). On fast-moving plates such as the Pacific, intraplate activity related to a long-lived mantle melting anomaly ("hotspot") typically results in a linear age progression of volcanic edifices such as the Hawaii-Emperor chain of islands and seamounts. Each of these is built during relatively short periods of volcanic activity (Clague & Dalrymple, 1987; Morgan, 1971). Moving away from the melting anomaly, the islands submerge below the water level. In the Atlantic Ocean, slower plate speeds lead to both a

Funding acquisition: Thor H. Hansteen, Ricardo S. Ramalho, Colin W. Devey
Investigation: Thor H. Hansteen, Ricardo S. Ramalho, Andreas Klügel, Lisa K. Samrock, Jo-Anne Wartho
Methodology: Tom Kwasnitschka, Colin W. Devey, Lisa K. Samrock, Jo-Anne Wartho
Project administration: Thor H. Hansteen, Ricardo S. Ramalho
Resources: Ricardo S. Ramalho, Jo-Anne Wartho
Software: Colin W. Devey, Jo-Anne Wartho
Supervision: Thor H. Hansteen, Ricardo S. Ramalho, Colin W. Devey, Jo-Anne Wartho
Validation: Thor H. Hansteen, Ricardo S. Ramalho, Colin W. Devey, Jo-Anne Wartho
Visualization: Tom Kwasnitschka
Writing – original draft: Tom Kwasnitschka
Writing – review & editing: Tom Kwasnitschka, Thor H. Hansteen, Ricardo S. Ramalho, Colin W. Devey, Andreas Klügel, Jo-Anne Wartho

more complicated age progression (Carracedo, 1999; Geldmacher et al., 2001) and a span of activity up to 25–40 Ma at any particular edifice (Geldmacher et al., 2005). Therefore, Atlantic hotspot volcanoes often exhibit very long but intermittent magmatic activity, characterized by more than one voluminous shield-building stage and often less voluminous post-shield stages (Carracedo, 1999; Geldmacher et al., 2001; Ramalho et al., 2010b, 2013, 2017; Ramalho, Helffrich, et al., 2010). Hotspot volcanism in the Atlantic is characterized by the interplay of thick and stiff lithosphere with strong buoyant hot spot swells. This leads to island evolutionary histories characterized by less subsidence when compared to Pacific or Indian Ocean linear island chains. It can even result in long-term uplift trends (Ali et al., 2003; Carracedo, 1999; Madeira et al., 2010; Ramalho et al., 2010a, 2010b, 2017; Ramalho, Helffrich, et al., 2010). However, the most poorly known aspects of oceanic intraplate volcanism are the submarine growth phases, notwithstanding the fact that these comprise a critical period in the formation of an ocean island as most of the island's volume lies underwater.

In this paper, we focus on the evolution of the Cabo Verde Archipelago, which is considered the type-example of an intraplate volcanic system with minimal movement of the plate (Burke & Wilson, 1972; Lodge & Helffrich, 2006; Sleep, 1990). Little is known about the numerous seamounts that make up the Cabo Verde Archipelago, and to what extent these seamounts either reflect or deviate from the evolutionary pattern observed in the adjacent volcanic islands. We use combinations of high-resolution multi-beam bathymetry, Remote Operated Vehicle (ROV) observations and sampling of rocks, to characterize the geomorphology of 12 major seamounts within the Cabo Verde Archipelago. Combinations of geomorphologic features reflecting growth and denudation processes are used to assign each seamount to an evolutionary stage, covering pre-shield, shield and post-shield stages and taking into account their spatial distribution across the archipelago. Supported by a new Ar/Ar-age for the easternmost Senghor Seamount, this comparative geomorphological study of the Cabo Verde seamounts aims to refine the inferred age progression within the archipelago. Further, we use the regional submarine geomorphology to shed light on the underlying geodynamic processes.

2. Regional Setting

Located between 14° and 18°N and 21°–27°W, 450–800 km off the West African coast, the Cabo Verde Archipelago resides on the largest geomorphological high of any ocean basin—the Cabo Verde Rise (Lancelot et al., 1978; Sleep, 1990). Its origin has been attributed either to the dynamic effects of a deep-seated and zoned mantle plume (Barker et al., 2010, 2012; Carvalho et al., 2019; Courtney & White, 1986; Holm et al., 2006; McNutt, 1988; Pim et al., 2008; Wilson et al., 2010, 2013) or the isostatic effects of a buoyant root of depleted melt-residue (Lodge & Helffrich, 2006; Ramalho et al., 2010a). The Cabo Verde Islands lie in the vicinity of the rotational pole of the African Plate (Pollitz, 1991), meaning that the oceanic crust moves slowly over any underlying magma sources. This results in both a weak and highly overlapping east-west age progression in different islands (Holm et al., 2008) throughout their long but intermittent magmatic lives (Ramalho, Helffrich, et al., 2010). Trace element and isotope signatures indicate a heterogeneous mantle source (Barker et al., 2012; Davies, 1988; Doucelance et al., 2003; Gerlach et al., 1988; Holm et al., 2006, 2008; Jørgensen & Holm, 2002; Mata et al., 2010, 2017; Plesner et al., 2002). The oldest known hotspot-related igneous rocks of the archipelago are exposed on the islands of Sal, Boavista, and Maio, K-Ar dated at 25.6 ± 1 Ma for Sal, and 16.3 ± 1.2 Ma for Boavista (Torres et al., 2002), and 19.3 ± 1.3 and 14.4 ± 2.0 Ma for Maio (Mitchell et al., 1983). Seafloor magnetic anomalies M0 - M16 (Müller et al., 2008) and results from nearby International Ocean Discovery Program sites (Faugeres et al., 1986; Lancelot et al., 1978) indicate that the archipelago lies on Mesozoic oceanic crust (140-120 Ma). Whether crustal fractures influenced the geometry of the archipelago is not clear (Williams et al., 1990). However, outcrops of Mesozoic MORB-type oceanic crust on Maio and Santiago suggest that vertical tectonics also played a role in the formation of the archipelago (Mitchell et al., 1983; Ramalho et al., 2010b; Ramalho, Helffrich, et al., 2010; Stillman et al., 1982).

Two chains of islands give the archipelago its "horseshoe" geometry. The southern chain (from NE to SW) consists of Sal, Boa Vista, Maio, Santiago, Fogo, and Brava (Figure 1). Fogo shows the only historical volcanic activity of any of these islands, erupting on average every 20 years since the islands were settled in the fifteenth century (Torres et al., 1997), the last eruption occurred in November 2014 to February 2015. Sal, Boa Vista and Maio are intensely eroded, being almost entirely razed by marine erosion and subsequently uplifted during the Quaternary (Ramalho et al., 2010a, 2010b; Ramalho, Helffrich, et al., 2010). Santiago, Brava and especially Fogo have much higher and steeper relief, while the Ilhéus Secos north of Brava comprise a number of cliffs only slightly above sea level. The northern chain (from ESE to WNW) consists of São Nicolau, Raso, Branco, Santa

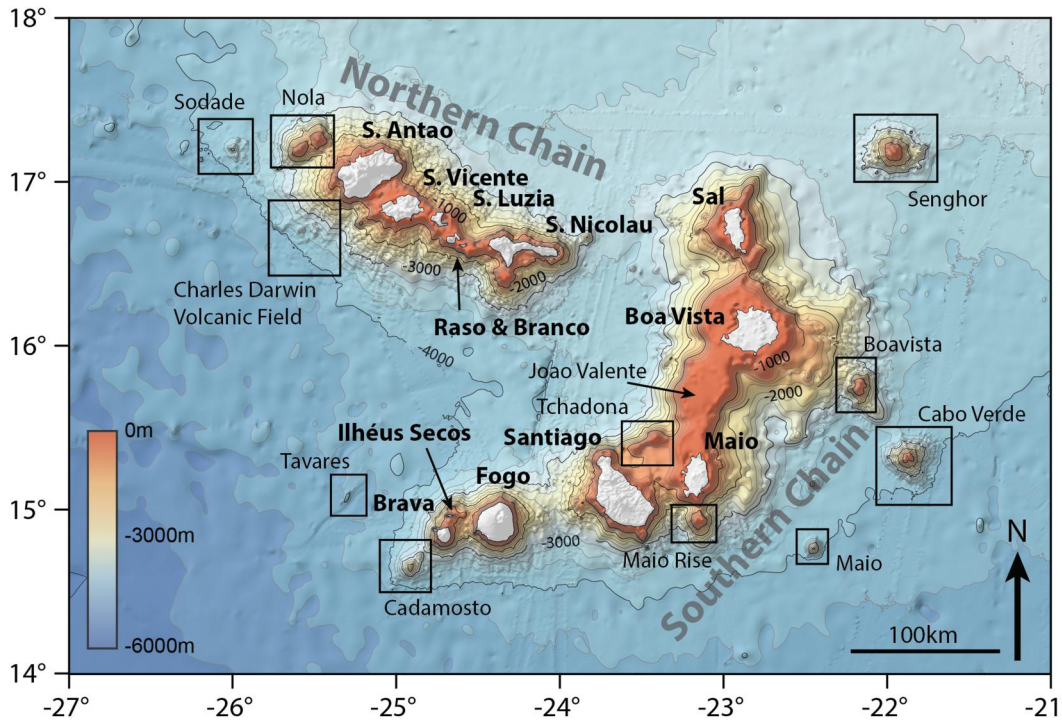

Figure 1. Global Multi-Resolution Topography map (Ryan et al., 2009) of the Cabo Verde Archipelago with the two main island chains marked as Northern and Southern Chains. Boxes mark the positions of the individual seamount maps. Islands are colored white, and their names are given in boldface. Color scales of all map figures are rounded to the next 100 m interval.

Luzia, São Vicente and Santo Antão. Comparatively recent volcanism occurs on all of these islands, with the youngest activity on Santo Antão recorded at ~90 ± 30 ka (Plesner et al., 2002), 57 ± 38 ka on São Nicolau (Duprat et al., 2007), and ~34–35 ka before present on São Vicente (Clemmensen & Holm, 2020). Frequent volcano-tectonic earthquakes are recorded offshore to the west of both island chains (Faria & Fonseca, 2014; Grevemeyer et al., 2009), possibly indicating current submarine volcanic activity.

With respect to island morphology, Santa Luzia and São Vicente show the effect of continued erosion deep into the island core but still have substantial relief (Ancochea et al., 2010). The islands of Santiago, São Nicolau and Santo Antão are deeply incised by erosion, but the general geometry of their volcanic shields is still evident. Fogo is an active stratovolcano with steep flanks and a large collapse scarp to the E, upon which a new edifice (Pico do Fogo) is growing, suggestive of a "somma-vesuvius" setting (Ribeiro, 1960). The island of Brava at the western end of the southern chain comprises an uplifted seamount covered by younger, largely felsic subaerial volcanic products in a post-erosional stage since 0.262 ± 0.005 Ma (Madeira et al., 2010). Seven km N of Brava, the small islands of Ilhéus Secos contain the remains of one or more eroded islands (Figure 1), but only residual morphologies now rise above sea level.

3. Previous Work on the Cabo Verde Seamounts

Previous studies of the Cabo Verde Seamounts and submarine geomorphology focused on the island slopes of the northern chain and the southwestern chain segments, where a number of slope failures were identified and the extent of their submarine deposits was mapped (Barrett et al., 2020; Le Bas et al., 2007; Masson et al., 2008). According to these studies, the dominant submarine features include: (a) landslide scars partly featuring erosional channels in their upper parts due to renewed volcanic activity after respective failure events; (b) proximal and distal deposits of debris flows including large-scale sediment waves and contour parallel sagging features; and (c) satellite volcanic cones on the submarine flanks, pedestals and upper slopes, of the main island edifices.

Initial dredge sampling of the Cabo Verde seamounts was undertaken on RRS CHARLES DARWIN cruise 85 (Hill, 1985). Particular attention was paid to the Cadamosto Seamount, which not only shows the most vigorous

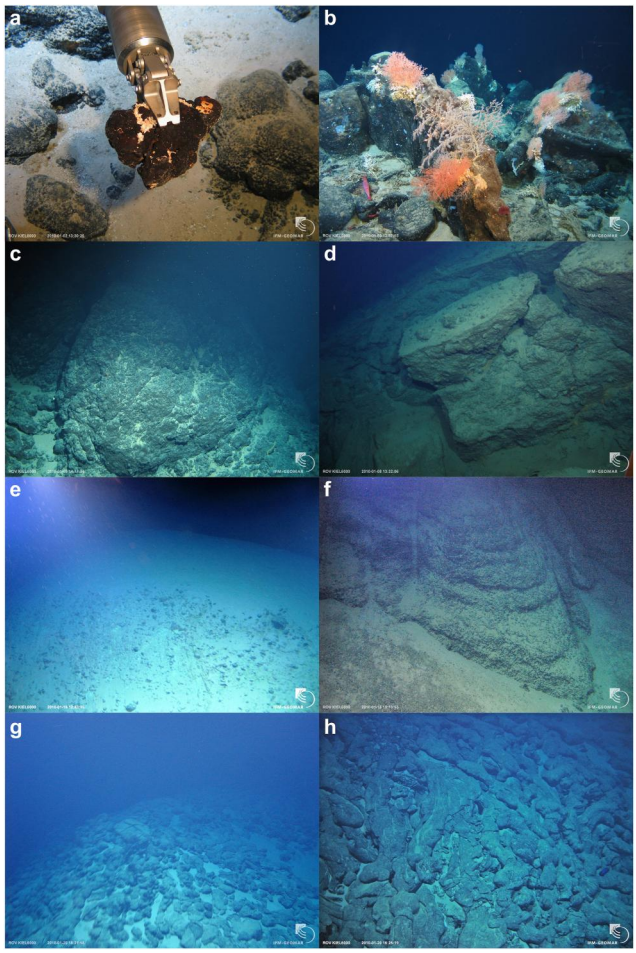

Figure 2. Photographs from Remote Operated Vehicle (ROV) KIEL6000 dives. (a) Senghor Seamount, showing thick manganese crusts that cover surface rocks at 341 m below sea level (mbsl). ROV gripper is 6 cm wide; (b) Lava-debris inside the S landslide scar of Cabo Verde Seamount at 880 mbsl, showing a vertical lava slab in the foreground. The rocks act as a substrate for black corals (*Hexacorallia*) and bamboo corals (*Isididae*). Shrimp for scale is about 12 cm long; (c) Cadamosto Seamount, showing large pillow lavas, probably of felsic composition, close to the SW summit crater at 1,530 mbsl. Field of view is about 3 m wide; (d) Cadamosto Seamount, showing a thick pyroclastic sequence on the flanks of the seamount at 1,456 mbsl. Field of view is about 5 m wide; (e) Kolá Seamount in the Charles Darwin Volcanic Field (CDVF), showing the outer flanks of the cone, close to its crater rim at 3,790 mbsl. The field of view is about 10 m wide; (f) Tambor Seamount in the CDVF, showing a thick, pyroclastic sequence exposed in the crater wall at 3,201 mbsl. Field of view is about 10 m wide; (g) Sodade Seamount, view over the summit of the main pillow ridge at 3,408 mbsl. Field of view is about 10 m wide; (h) Sodade Seamount showing a pillow lava sequence on its W flank at 3,605 mbsl. The field of view is about 5 m wide. Additional photographs are provided in Supporting Information S1.

seismic activity of the whole archipelago (Grevemeyer et al., 2009) but is largely composed of phonolitic rocks. This is in contrast to the mafic volcanism that dominates most of the Cabo Verde islands (Barker et al., 2012), with the exception of Brava, which is located near the Cadamosto Seamount (Figure 1; Madeira et al., 2010). In contrast to the islands, no radiometric ages have yet been obtained for the submarine edifices of the Cabo Verde, except for the seismically active Cadamosto Seamount, which yielded ^{40}Ar-^{39}Ar phenocryst eruption ages ranging from 21.40 ± 0.63 to 97 ± 14 ka (Samrock et al., 2019).

4. Methods

4.1. Acoustic Data Acquisition and Processing

The data presented in this study are primarily based on multibeam swath bathymetry and backscatter data gathered over 18 years, from five cruises: (a) CHARLES DARWIN 168 (CD168) focused on slopes and foothills of the northern chain using a hull-mounted Kongsberg EM12 echo sounder (Masson et al., 2008)). (b) R/V METEOR 62/3 (M62/3) focused on the southern chain between Santiago and Brava using a hull-mounted Atlas Hydrosweep echo-sounder. (c) R/V METEOR 79/3 (M79/3) focused on Senghor, Boavista and Cabo Verde Seamounts, and Charles Darwin Volcanic Field (CDVF) using a hull-mounted Kongsberg EM 120 echo-sounder, plus a Sub-Atlantic Mohawk Class ROV on the summit and upper flanks of Senghor Seamount at a depth of 700 m). (d) R/V METEOR 80/3 (M80/3) focused on Maio Rise, Senghor, Boavista, Cabo Verde, Maio, Cadamosto, Tavares, Nola and Sodade Seamounts, including most transits, using the same echo-sounder as M79/3, plus the GEOMAR Schilling ROV Kiel6000 was used to provide video coverage (Figure 2, Text S1 in Supporting Information S1) and collected rock samples from volcanic edifices between 600 and 4,000 m depths from the Senghor, Cabo Verde, Cadamosto, and Nola Seamounts, Maio Rise and the CDVF. (e) NRP GAGO COUTINHO used hull-mounted Kongsberg EM 120 and Kongsberg EM 710 echo sounders covering Tchadona Seamount.

These regions were mapped at a resolution of 10–100 m, depending on the average water depth, which varied from 60 to 3,000 m. Backscatter data (M79/3 and M80/3) were processed using QPS FMGT and merged with existing maps of the M62/3 and CD168 cruises (see Text S2 in Supporting Information S1).

4.2. ^{40}Ar-^{39}Ar Dating

Total-fusion ^{40}Ar-^{39}Ar laser dating was undertaken on single crystals of K-feldspar and biotite from one volcaniclastic sample (M79/3 950/2) located at 17° 09.94′N22° 06.83′W on the flank of Senghor Seamount at a depth of 3,018 mbsl (Christiansen et al., 2011). All ages are quoted with 2σ errors, unless otherwise stated. Further details of the ^{40}Ar-^{39}Ar dating method can be found in Samrock et al. (2019) and Text S4 and S5 in Supporting Information S1. The data were processed using a total 40 K decay constant of 5.543 (±0.009) × 10^{-10} years, and a Taylor Creek sanidine age of 28.344 ± 0.011 Ma (1σ; Fleck et al., 2019). To allow direct comparison between previous literature ^{40}Ar-^{39}Ar ages using this relative dating technique (relative to standards ages), all ^{40}Ar-^{39}Ar ages in this manuscript have been recalculated by an author-written (J-AW) program using a total 40 K decay constant of 5.543 × 10^{-10} years, and the Taylor Creek sanidine and Fish Canyon biotite/sanidine standard ages of Fleck et al. (2019).

4.3. ROV Observations and Sampling

The Cabo Verde seamounts cover a broad range of rock compositions spanning from primitive nephelinites, foiditites and basanites to phonolites, and include lavas and pyroclastic rocks (Barker et al., 2012, 2019; Hansteen et al., 2014). Photographs of rock outcrops were acquired during all the ROV dives during the M80/3 cruise and used to illustrate the nature of the seamounts (Figure 2). Rock samples were collected by the ROV manipulator arms (Figure 2a), and by dredging the seamount flanks. For the purpose of this paper, we refer to the compositions of the sampled lavas, dikes and pyroclastic rocks using the general terms basaltic, phonotephritic/tephriphonolitic, and phonolitic as determined by description of hand specimens. Phonolitic rocks were distinguished using alkali feldspar as an index mineral.

5. Results

5.1. Description of Seamount Bathymetry and ROV Observations

5.1.1. Senghor Seamount

Senghor Seamount (also referred to as Nova Hollanda; e.g., Freitas et al., 2018) lies ∼100 km E-NE of Sal and rises to a depth of just 93 m mbsl, and marks the NE limit of known volcanic activity in the Cabo Verde Archipelago (Figures 1 and 3). From the base of Senghor seamount at about 3,000 mbsl up to 1,500 mbsl, a large number of well-developed circular and compound satellite cones between 0.5 and 2 km in diameter can be found in all sectors. The summit forms an oval NNW-SSE oriented flat top plateau with very little relief at about 100 mbsl. Intercalated patches of low backscatter at the summit (Figure S2.1 in Supporting Information S1) were identified as carbonate sand on M79/3 ROV dives (Christiansen et al., 2011). The plateau edges break off in steep slopes with their foothills dominated by sedimentary talus fans covering large portions of the hummocky volcanic plateau at ∼500 mbsl (Figure 3).

Senghor lacks large-scale mass wasting scars, but its entire W flank exhibits a graben-like depression at depths between 500 and 1,000 mbsl, which may be due to either erosion or to subsidence (Figure S3.1 in Supporting Information S1).

The seamount flanks display ridges surrounded by erosional valleys, with the two most prominent ridges extending to the ENE. Samples obtained from dredges and ROV contain strongly altered basaltic to phonolitic volcaniclastic material and blocks of lava flows coated with manganese crusts of up to 9 cm thickness. ROV video coverage of the lower slopes (Figure S3.1 in Supporting Information S1) confirmed the ubiquitous layer of manganese crust on most hard substrates (Figure 2a). Radiometric age dating on a rock from Senghor Seamount is presented later in Section 5.2.

5.1.2. Boavista Seamount

Boavista Seamount, which is incised by deep erosional channels, lies along the SE slope of Boavista Island. The edifice has a maximum basal diameter of 24 km and rises from its foothill at 3,000–400 mbsl, where it forms an extensive double plateau separated by a 3 km wide saddle-like valley (Figure 4). The volcanic edifice is strongly incised by four large-scale flank collapse scars. In the W, a number of satellite cones are observed on the non-collapsed flank between 1,500 and 3,000 mbsl.

The debris fans on the foothills of the SW, W and N slope collapse scars display low (dark) acoustic backscatter (Figure S2.2 in Supporting Information S1), suggesting considerable post-collapse sedimentation and a lack of post-collapse volcanism in these areas. The flank collapse headwalls are incised by smaller gullies. A failure on the NE flank shows lesser amounts of slip, with a large debris fan within the lower scar, while the respective segment of the summit plateau merely has a steep scarp (Figure 4). The SE flank remained partly intact, and was only locally mobilized, as shown by a number of arcuate downslope faults.

5.1.3. Cabo Verde Seamount

Cabo Verde is a large solitary seamount 150 km E of Maio Island (Figure 5). With a basal diameter of 35 km outlined by the 3,900 mbsl contour, it rises to its summit at 511 mbsl. At a radius distance of ∼9 km from the summit (between ∼3,500 and 2,000 mbsl), numerous satellite cones line its flanks. Above the 1,000 mbsl depth

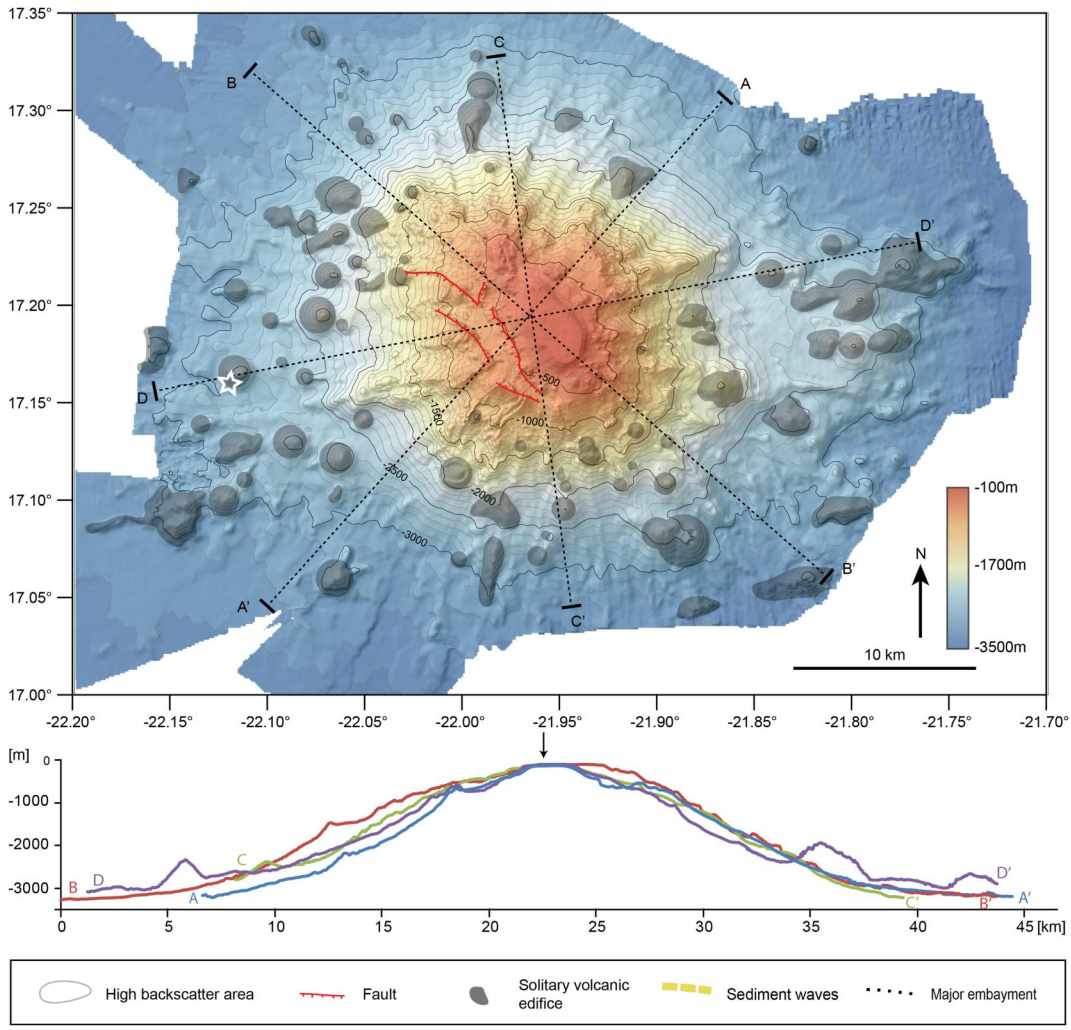

Figure 3. Geomorphologic map of Senghor Seamount with 2x exaggerated cross sections. Note the elongated graben structures present on the W sector, and the flat top of the seamount. The white star indicates the location of ^{40}Ar-^{39}Ar dated sample (M79/3 950/2). The legend presents all features observed throughout Figures 3–11.

contour, hummocky relief with 280 m undulations covers the summit plateau (with a radius distance of 2.5 km), which we tentatively identify as aligned volcanic centers.

The seamount is dissected on the S and N slopes by two conspicuously long and deep valleys, striking NNW-SSE. The S valley reaches all the way into the central summit area, terminating in a semi-circular depression of 1.2 km diameter and 220 m depth below the surrounding terrain. A ROV transect into the S valley revealed an exposed composite volcanic succession comprised of submarine lava flows, pyroclastic sequences and crosscutting dykes (Figure 2b and Figure S3.2 in Supporting Information S1). The W and E flanks are lined with erosional channels corresponding to high backscatter areas exposing smaller radial ridges (Figure S2.3 in Supporting Information S1). A succession of sediment waves was observed in the E and SE foothills between 3,800 and 4,000 mbsl.

Rock samples dredged near the S scar (015 DR & 016 DR, Figure S3.2 in Supporting Information S1) dominantly comprise basaltic to intermediate lavas and hyaloclastites of varying grades of alteration, with a coating of manganese crust up to several centimeters thick.

5.1.4. Maio Seamount

Maio Seamount has the comparatively simplest structure of all seamounts at Cabo Verde (Figure 6). Situated 90 km SE of Maio Island, it rises from a relatively flat seafloor and is devoid of any peripheral volcanic centers. Its

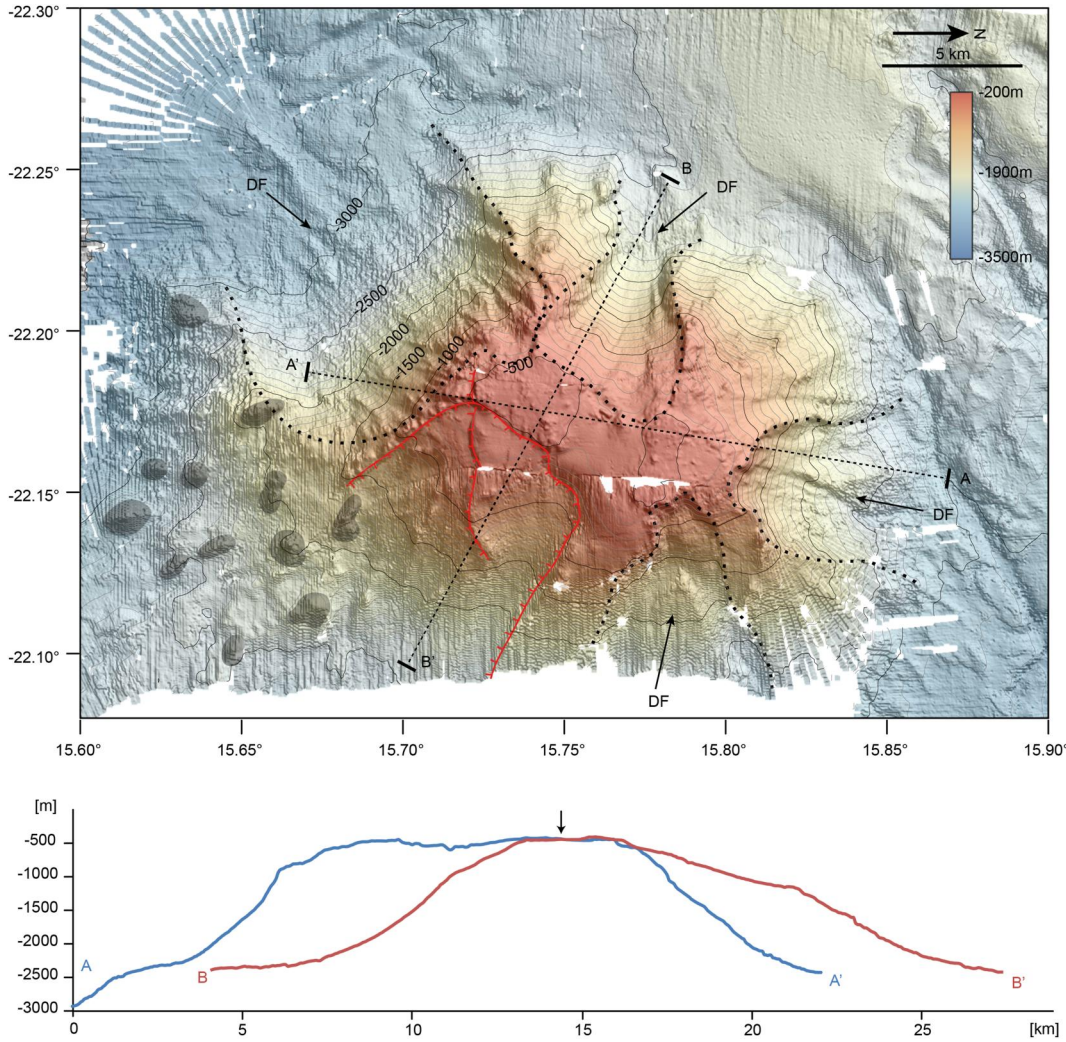

Figure 4. Geomorphologic map of the Boavista Seamount including 2x exaggerated cross sections. Note the large collapse scars that modify the volcanic edifice and their debris fans (DF) marked by arrows. Arrow marks intersection of the cross-sections.

basal diameter is 20 km, and it has a radially symmetric cone that rises 2,100 m above the 4,000 mbsl isobath. Small channels (less than 500 m wide) line its flanks running down the slopes to its foothills. Lines of high backscatter at the foothills end in small patches (Figure S2.4 in Supporting Information S1), which likely represent erosional fans.

The main striking feature is a ridge bisecting the Maio Seamount from NNE to SSW. In the upper flanks, the ridge appears to bifurcate forming elongated troughs. Near the summit, there is a 1,000 m wide depression, which opens toward the N forming a narrow and elongated feature that may represent a landslide scar. Dredging across the summit yielded thick crusts of manganese oxides but only marginally altered volcanic rock samples (Figure S3.3 in Supporting Information S1).

5.1.5. Maio Rise

Maio Rise (Figure 7) is located on the S submarine flank of Maio Island, has a basal diameter of 24 km and rises from 3,000 to 300 mbsl. It has a summit plateau 6 km in diameter that is flat in the center and exhibits a low hummocky morphology with very low backscatter (Figure S2.5 in Supporting Information S1), indicating sediment cover. There is no sign of obvious morphological terraces around or within the plateau.

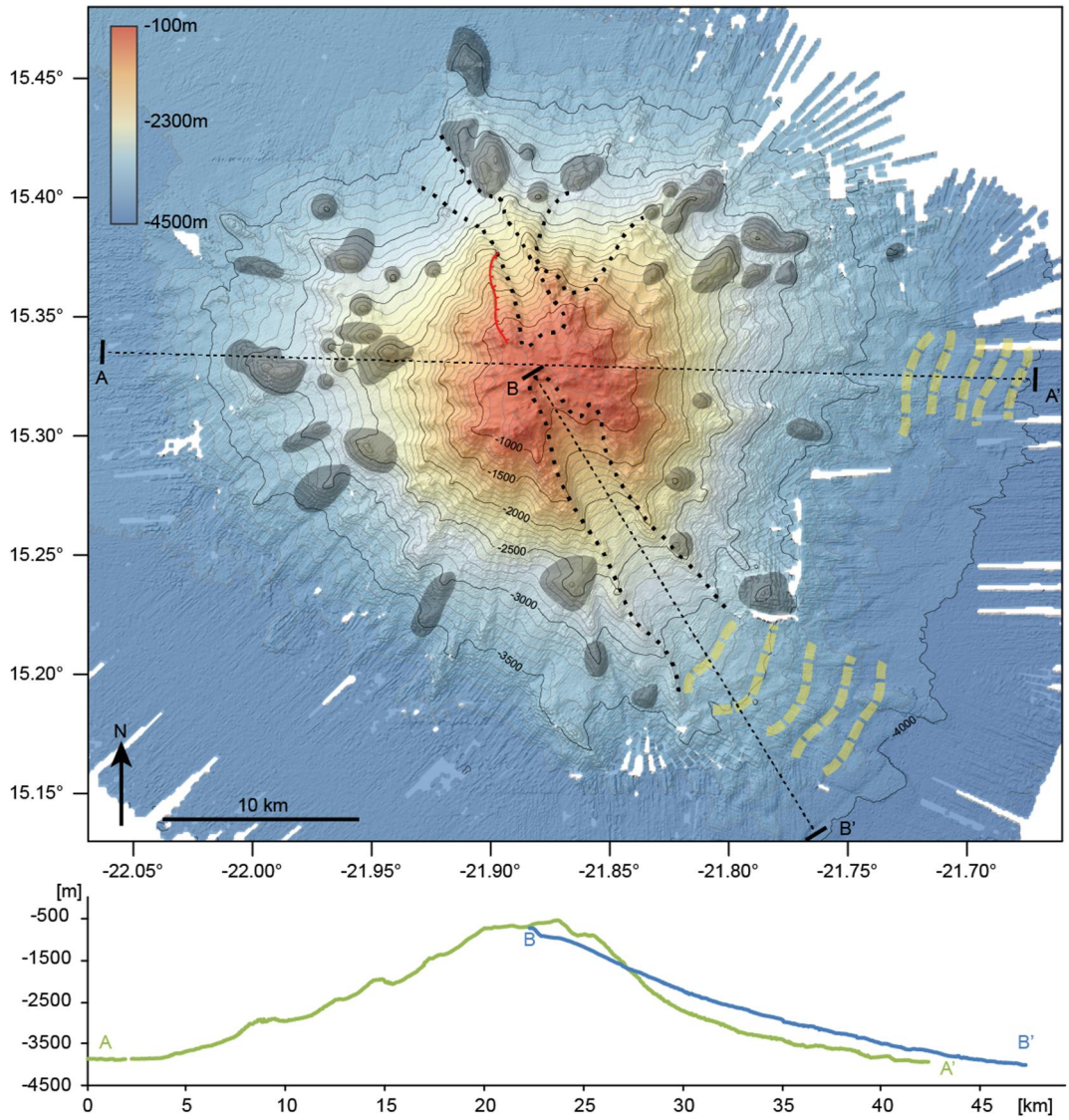

Figure 5. Geomorphologic map of Cabo Verde Seamount including 2x exaggerated cross sections. Note the two elongated valleys that fan to the NW and SE from the summit. A Remote Operated Vehicle dive into the SE valley displayed well-developed headwall scars, demonstrating that the valleys represent collapse structures. The SE and E flanks exhibit sediment waves in their lower sectors.

The volcano exhibits shield-like flanks, with partly irregular morphology due to three obvious landslide scars, and only a few satellite cones occurring between 3,000 and 1,500 mbsl. The three major collapse scars dominate the relief in the N, NE and S sectors. The NE scarp exposes a steep headwall, but a debris fan is not evident from the bathymetry. Dredged samples (Figure S3.4 in Supporting Information S1) yielded moderately to heavily altered basaltic to intermediate rock fragments with a manganese crust up to 5 mm thickness as well as volcaniclastic breccia of basaltic-intermediate clasts with carbonate-filled vesicles.

5.1.6. Tchadona Seamount

Tchadona Seamount (Figure 8) is located on the upper WNW flank of Maio Island, and is part of the submarine platform extending from Maio to N of Santiago Island (Figure 1). The asymmetric and elongated structure has a basal diameter of ~30 × 15 km and rises from ~2,500 to 30 mbsl. The shallow, smooth E summit plateau has the greatest width of 6 km, while the W summit area at ~300 mbsl features a hummocky morphology. The slopes toward the ENE and NW are comparatively intact with only minor landslides, whilst a series of sharp along-strike

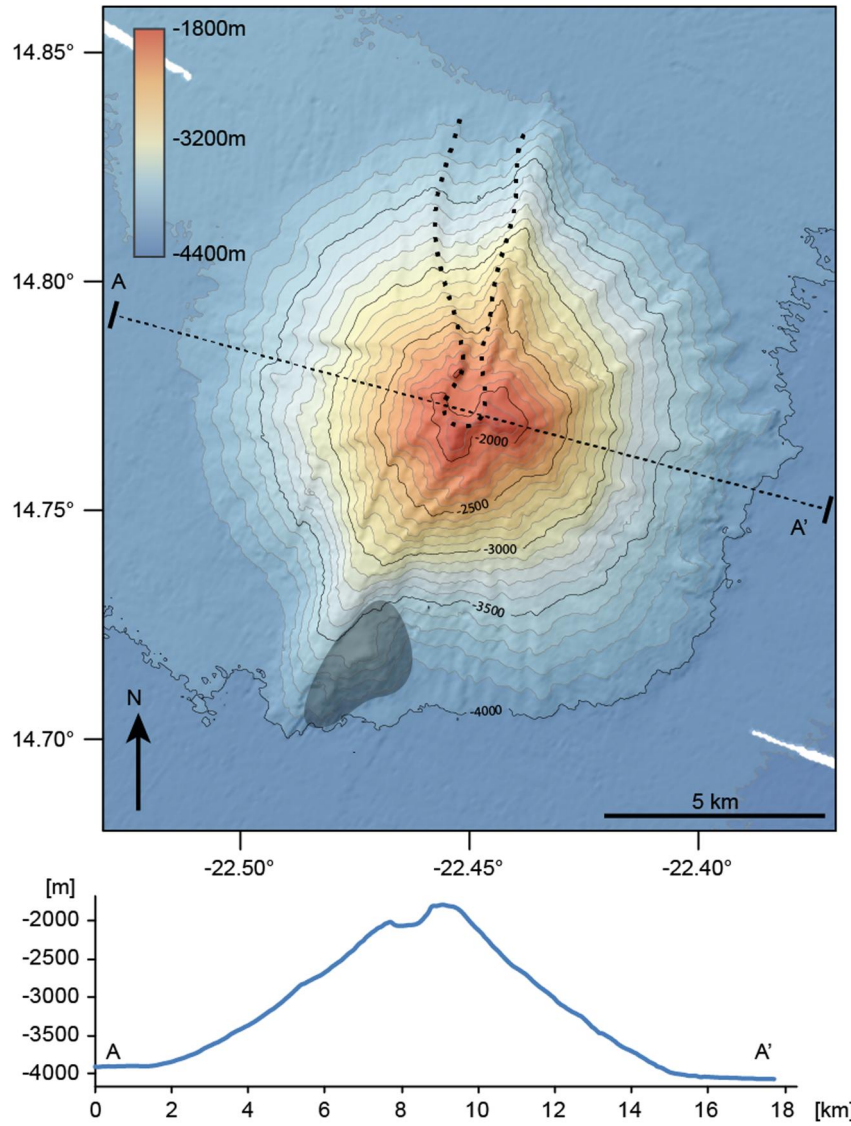

Figure 6. Geomorphologic map of Maio Seamount including a 2x exaggerated cross section.

erosional cliffs dominate the S flank, extending toward Maio island. An opposite, broad erosional embayment opens on the NNW flank toward the Cabo Verde Basin. The comparatively undisturbed ESE and W flanks exhibit a number of elongated to circular satellite cones.

5.1.7. Cadamosto Seamount

Cadamosto Seamount rises from 4,000 to 1,500 mbsl with a basal diameter of ~30 km. A field of isolated mounds, interpreted as volcanic cones, is situated on the saddle between Cadamosto and Brava Island to the NE. A limited number of smaller cones occur on the lower flanks (Figure 9), indicating dispersed magmatic activity in a wide area surrounding the seamount.

The N and W flanks are characterized by a radial system of embayments and hummocky ridges. The upper slopes of the embayments show a number of smaller channels and gullies whereas the lower two thirds are very smooth (Figure 9b), suggesting a comparatively high amount of mass wasting (Figure S2.6 in Supporting Information S1).

The SW sector is much more rugged and is likely to be affected by slumping with debris avalanche deposits between 2,000 and 2,500 mbsl. A possible debris fan stretches from the foothill of the slump down to the 3,600

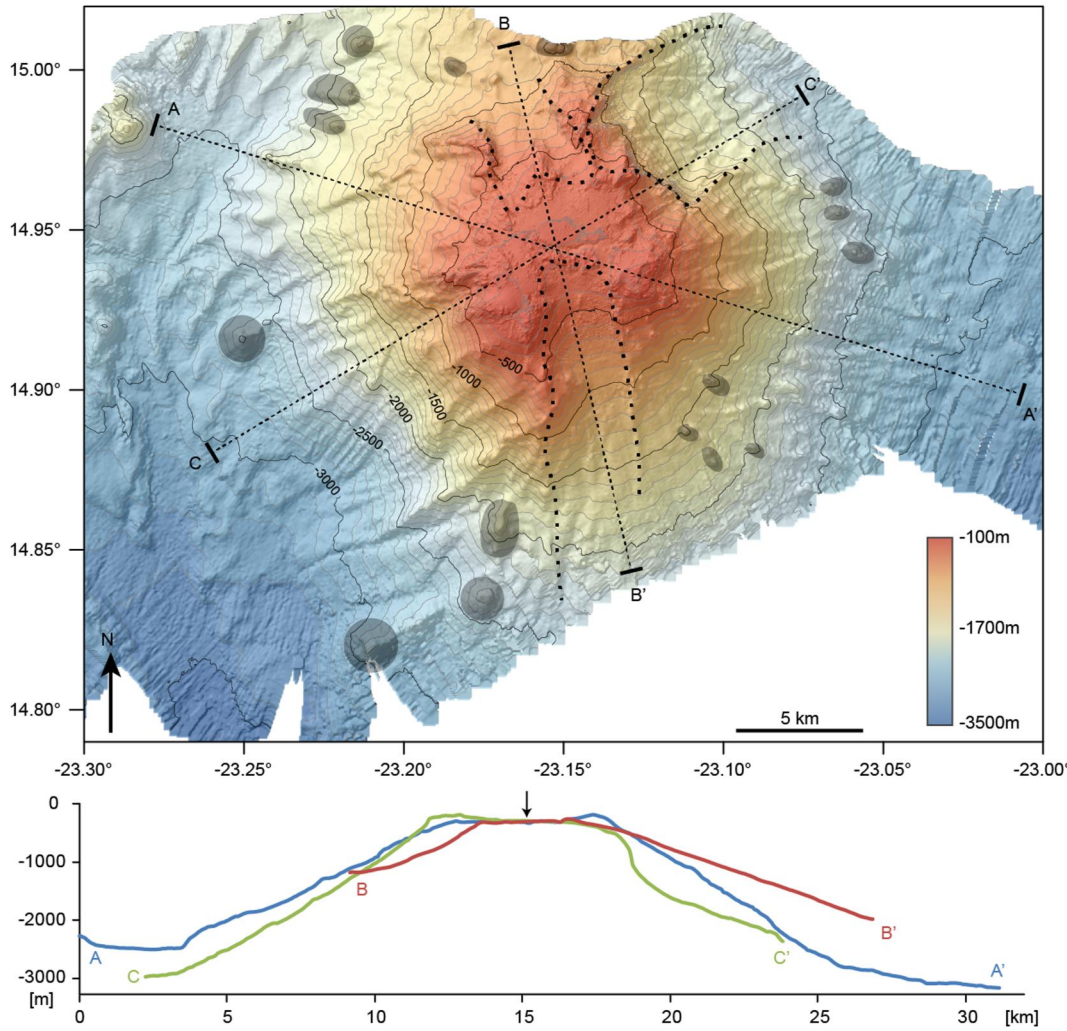

Figure 7. Geomorphologic map of Maio Rise including 2x exaggerated cross sections. Arrow marks intersection of the cross-section.

mbsl contour. Two clearly visible slumps occurred on the S sector, with well-exposed headwalls and their talus bodies forming terraces on the slope. ROV images show that the summit contains several pit craters and large pillow and sheet lava flows with no pelagic sediment cover, thus suggesting a young origin (Figures 2c and 2d). Fresh ROV-samples of lava flows are black to gray and partly glassy with local patchy alteration (Figures S1a and S3.5 in Supporting Information S1). The lavas are dominantly phonolites (Samrock et al., 2019). Dredge samples of the cone field between Cadamosto and Brava are also phonolitic to phonotephritic (Samrock et al., 2019), and are chemically similar to the <262 ka phonolitic eruptions on Brava (Madeira et al., 2010; Mourão et al., 2012). The summit area comprises at least four eruption centers, two of which were identified by ROV dives (Figure 9b; Hansteen et al., 2014). Samples from the inner crater walls and crater floors locally show yellowish to brownish patches of altered rocks, indicating hydrothermal alteration. Seismic data strongly indicate that Cadamosto is an active volcano (Faria & Fonseca, 2014; Grevemeyer et al., 2009).

5.1.8. Tavares Seamount

When this seamount was reviewed prior to the cruise, coarse bathymetry data inferred from satellite altimetry data (Smith & Sandwell, 1997; www.gebco.net) indicated two seamounts W and WNW of Brava Island. Our bathymetry data show that only the WNW feature (named Tavares) corresponds to a pronounced seamount, the other probably constituting an artifact.

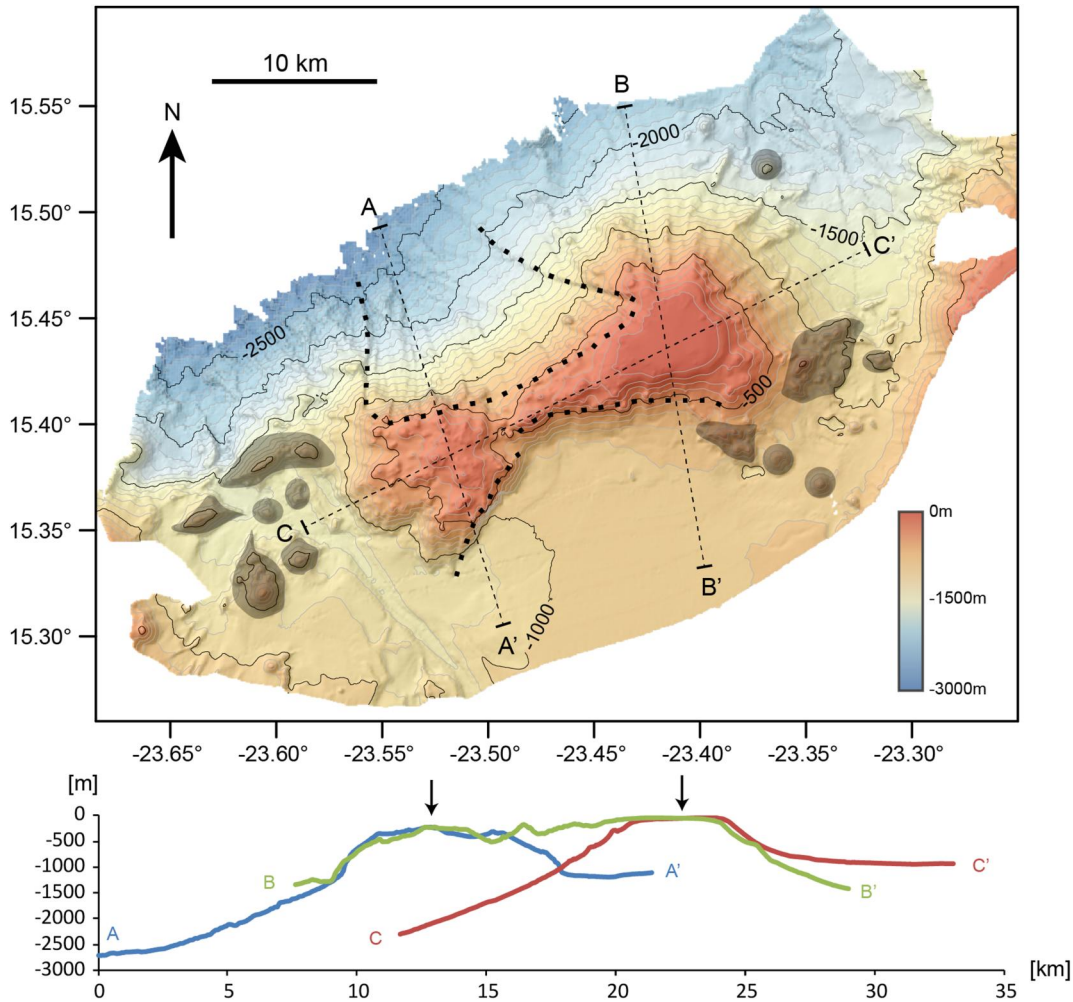

Figure 8. Geomorphologic map of the Tchadona Seamount including 2x exaggerated cross sections. Arrows mark intersections of the cross-sections.

Tavares is a narrow, curved volcanic ridge of 12 km length, up to 3 km wide and 500 m high rising from a depth of 4,200 mbsl. It is situated at the tip of a 7 km wide and more than 30 km long plateau with a pronounced edge along its E margin (Figure 10). At the SW end of this plateau, ~25 km away from the main seamount, there is a small bifurcating ridge. We interpret the steep E flank of the plateau to represent the rim of an asymmetric SW-striking sediment flow channel (Figure S2.7 in Supporting Information S1), which indicates heavy sedimentation from the basin between the northern and southern Cabo Verde chains.

Both Tavares and the SW ridge feature pronounced positive gravity anomalies (Jena et al., 2012; Smith & Sandwell, 1997), which are best explained by the presence of local intrusive rocks. These gravity anomalies are thus responsible for the "relief" shown in the earlier Ryan et al. (2009) bathymetry study (Smith & Sandwell, 1997). Tavares Seamount and the underlying ridge show no visible signs of peripheral volcanic activity or a connection to nearby volcanic complexes.

5.1.9. Nola Seamounts

Nola (also referred to as Noroeste in local maps and charts; Samrock et al., 2019) is described in the literature (Masson et al., 2008; Monteiro et al., 2008) as a single seamount with a twin peak. However, detailed mapping reveals that it contains two seamounts, which coalesce at the base forming a saddle at a depth of 1,200 mbsl (Figure 11). We therefore refer to these seamounts as Nola East and Nola West. Their common base at 3,500 mbsl is elliptical with a maximum diameter of 40 km.

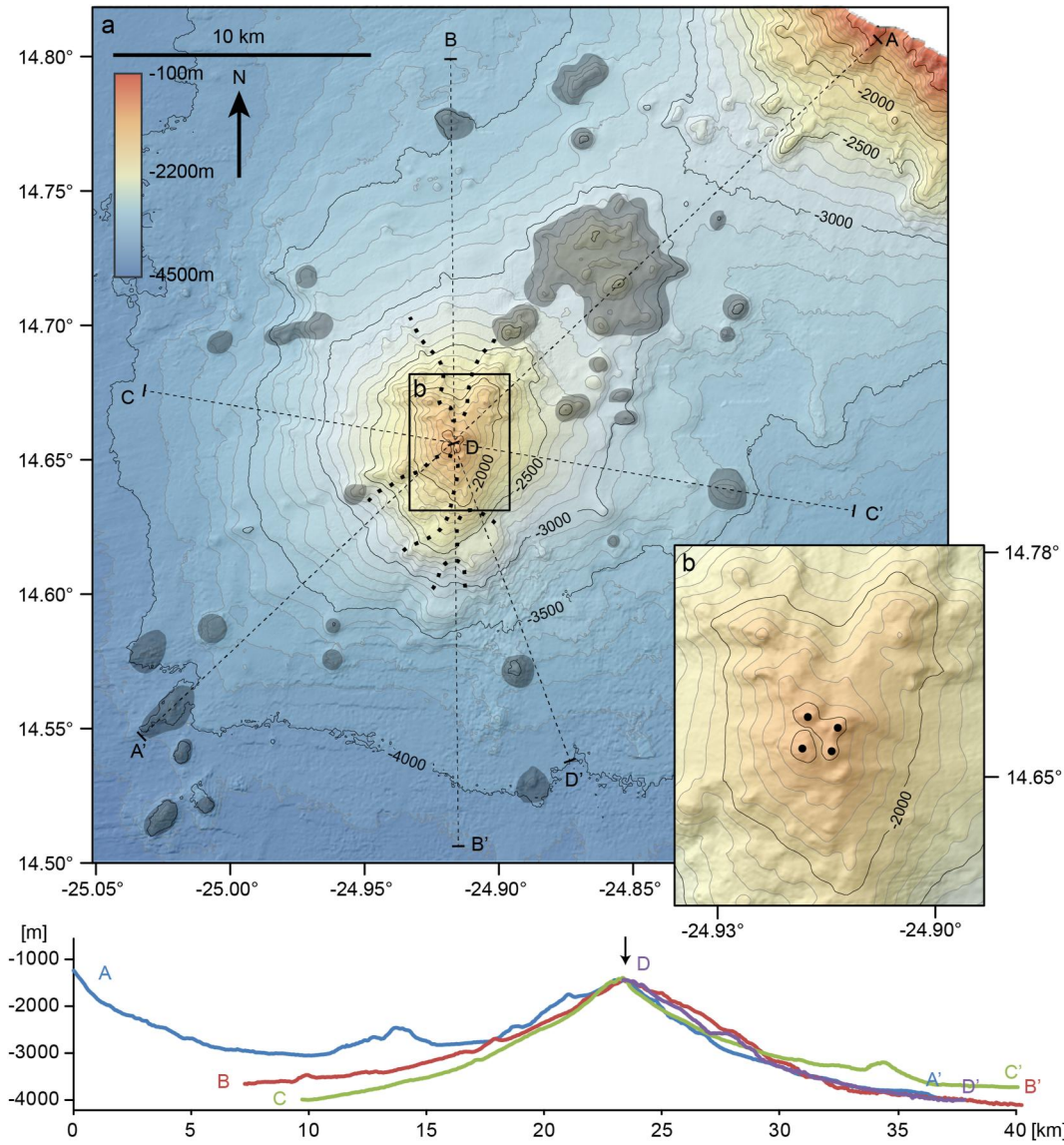

Figure 9. (a) Geomorphologic map of Cadamosto Seamount including 2x exaggerated cross sections. Arrow marks intersection of the cross-sections (b) close-up of the summit region showing assumed eruption centers (black circles).

Both summits form flat elliptical plateaus, which are as shallow as 35 mbsl. They show dark patches of back-scatter (Figure S2.8 in Supporting Information S1) analogous to those seen at Senghor, but also steep residual morphologies interpreted as volcanic necks. Both plateaus have steep flanks that transition into a clear morphological terrace at ~200 mbsl. Below 500 mbsl, both seamounts display a number of small hummocks separated by valleys of probable erosional nature, which create complex relief. Slope failures have incised the NE and SW slopes of Nola East.

ROV and dredge samples of peripheral cones on the SW lower flank (DR81) yield partly altered basaltic pillow fragments, carbonate-cemented volcaniclastics and scoria fragments (Figure S3.6 in Supporting Information S1). The upper slope of Nola East yield basaltic, vesicular lava fragments with millimeter-thick manganese crust coatings. Nola West has occurrences of basaltic lavas and pyroxenitic cumulates coated by manganese crusts.

5.1.10. Charles Darwin Volcanic Field

The CDVF is situated off the SW slope of Santo Antão island, at depths between 4,000 and 3,000 mbsl. The field consists of 13 major single or compound volcanic cones (Figure 12), and comprises basanitic, foiditic and

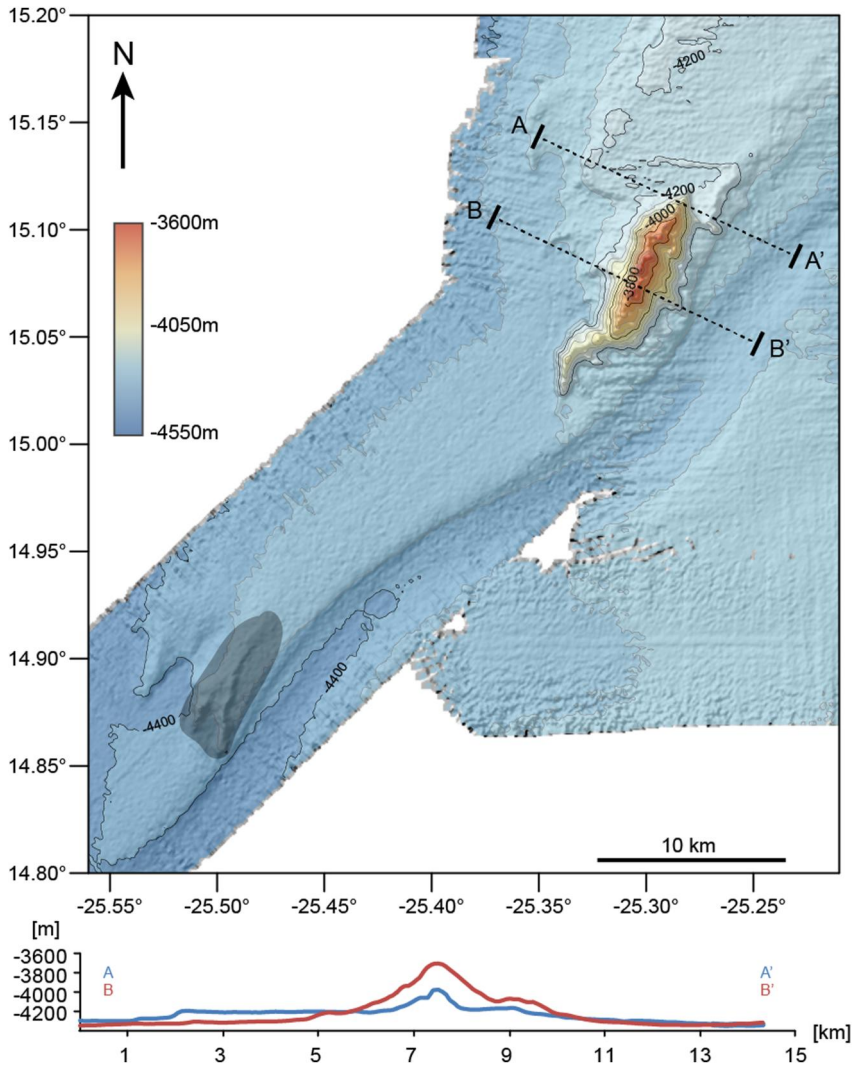

Figure 10. Geomorphologic map of Tavares Seamount including 2x vertically exaggerated profiles.

phonolitic rocks, many of which have glassy groundmass. Most of the volcanoes have a circular cone-shaped geometry, with Tambor and Batuku exhibiting well-exposed summit craters. Tambor and Batuku have constructive morphologies relative to the surrounding terrain; the latter is covered by two morphologically young cones. In contrast, Kolá is a morphological depression about 1 km wide within a group of smaller volcanic cones. The craters of Tambor and Kolá are wide and comparatively shallow, exhibiting nearly vertical walls with well-exposed pyroclastic sequences (Figures 2e and 2f), and are characterized by flat crater floors. The Tabanka group reveals a succession of eruptive activity, with its four eruption centers mutually overlapping each other.

All structures are covered by up to 0.5 m thick pelagic sediment (foraminiferal ooze) verified during ROV dives (Figure S3.7 in Supporting Information S1). Sediment waves surround the CDVF, and partly occur between the eruption centers. The central part of the CDVF between Tabanka, Batuku and Mandora is covered by a deposit with high backscatter, sharp boundaries, and lobate downhill flow patterns that correlate with a hummocky field of lava flows found by ROV. The lavas seem to drape over the sediment waves, and thus CDVF may postdate the slope failure events of W Santo Antão, which have been assigned ages of ∼>200 ka (Holm et al., 2006; Masson et al., 2008).

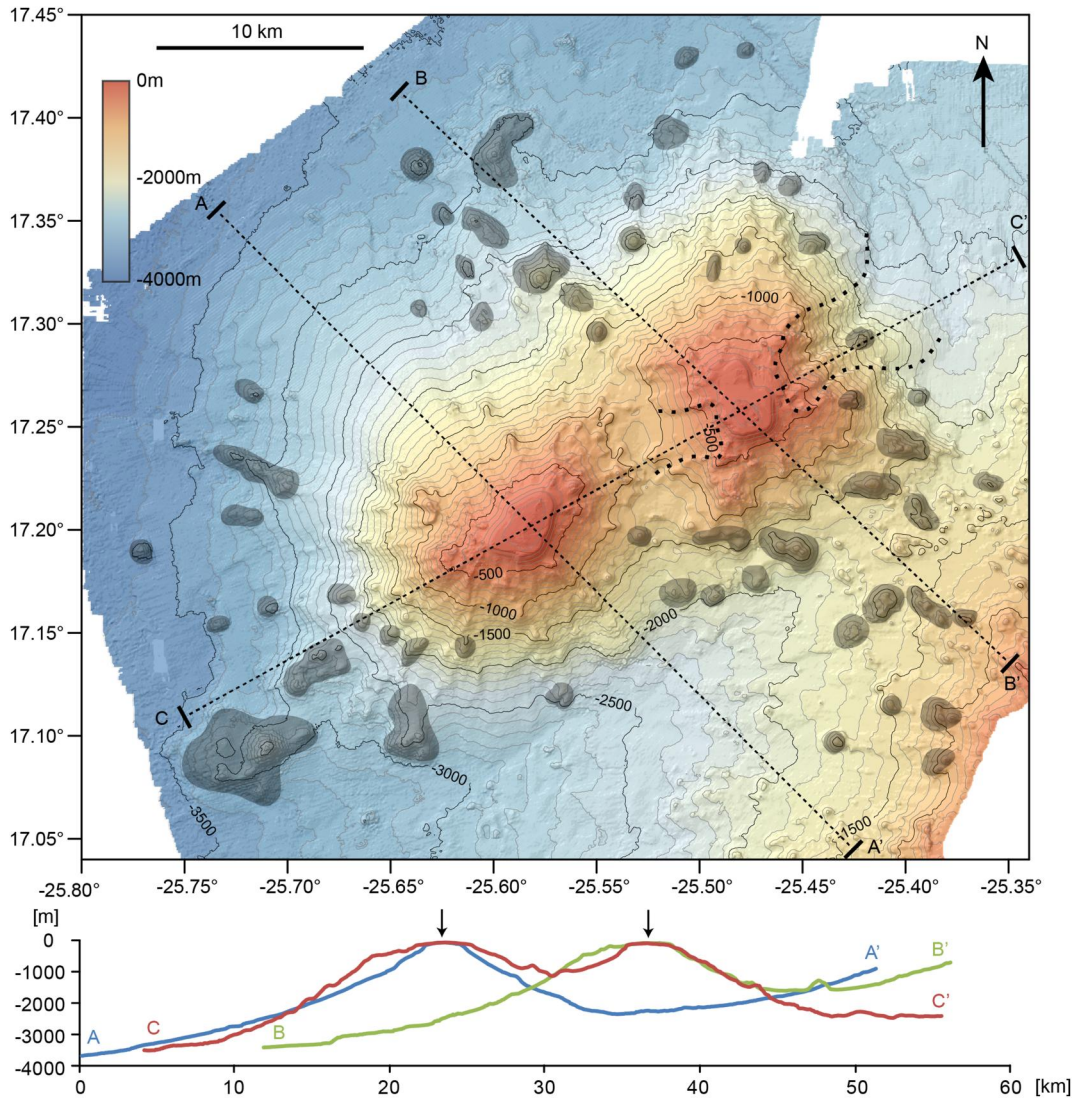

Figure 11. Geomorphological map of Nola Seamounts including 2x exaggerated cross sections. Arrows mark intersections of the cross-sections.

5.1.11. Sodade Seamount

Sodade Seamount, rising 1,100 m above the seafloor at 4,000 mbsl, was identified during our investigation of another Global Multi-Resolution Topography gravity anomaly (Ryan et al., 2009), and is located ~40 km W of Nola, resting on a foothill of 15 km basal diameter. Our ROV observations indicate mostly pillow lavas and other effusive structures (Figures 2g and 2h; Figure S3.8 in Supporting Information S1). A dozen satellite cones lie within a radius of 5 km from the summit, lining the entire perimeter except for the NW sector (Figure 13). Three cones with obvious crater structures are recognized directly to the NE and 4 km SSE of the summit. The main edifice shows a steep morphology with a number of arcuates, spinal-shaped ridges leading to the summit. The area surrounding the seamount is characterized by high backscatter (Figure S2.10 in Supporting Information S1), and comprises lobate downhill flow structures toward the W lower flank. Analogous to the CDVF, this area is interpreted to be covered by young volcanic deposits owing to the thin cover of pelagic sediment.

An ROV transect of the W flank showed that Sodade largely consists of pillow lavas (Figure S1d in Supporting Information S1). Samples yielded glassy mafic alkaline pillow fragments. Manganese crusts cover some of the NE peripheral cones, as confirmed by dredging.

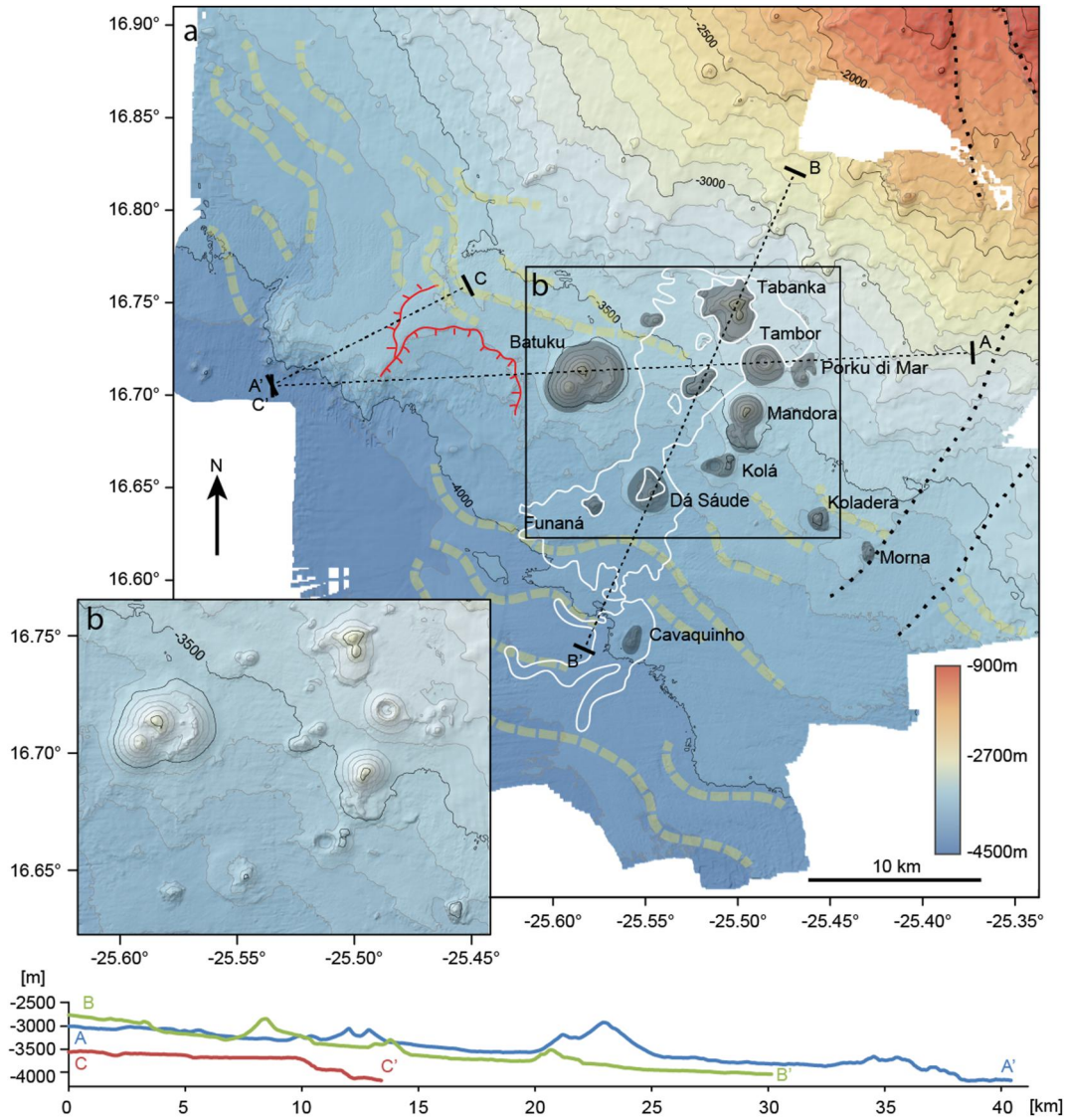

Figure 12. Geomorphological map of the Charles Darwin Volcanic Field and 2x height exaggerated sections. White outlined area indicates high-backscatter areas (Figure S02.9 in Supporting Information S1).

5.2. ^{40}Ar-^{39}Ar Dating at Senghor Seamount

A volcaniclastic sample from Senghor Seamount (M80/3 950-2) comprising various rock clasts and mineral grains was used for ^{40}Ar-^{39}Ar dating. Seventy single- or multi-crystal laser total-fusion ^{40}Ar-^{39}Ar analyses were undertaken on both K-feldspar (n = 36) and biotite (n = 34) crystals. A summary of our results is presented in Table 1, and all the tables and plots are shown in Supporting Information S1.

The M80/3 950-2 single-/multi-crystal biotite ^{40}Ar-^{39}Ar analyses yield a weighted mean age of 14.901 ± 0.034 Ma (Mean Square Weighted Deviation (MSWD) = 0.67, Probability (P) = 93% n = 34). The same data give an inverse isochron age of 14.911 ± 0.042 Ma (95% confidence (conf.), MSWD = 0.67, P = 92%), with an initial ^{40}Ar/^{36}Ar ratio of 293.9 ± 4.1 that is within 95% conf. errors of the atmospheric ^{40}Ar/^{36}Ar ratio of 295.5, and has an acceptable Spreading Factor (SF) value of 57%.

The M80/3 950-2 single-crystal K-feldspar ^{40}Ar-^{39}Ar analyses yield a weighted mean age of 14.861 ± 0.029 Ma (MSWD = 1.15, P = 25%) from n = 36 analyses, that overlaps within 2σ errors with the biotite weighted mean age (Table 1). The inverse isochron age from these 36 analyses gives an age of 14.841 ± 0.033 Ma (95% conf., MSWD = 0.99, P = 48%) that overlaps within 2σ errors with the weighted mean age. The inverse isochron plot

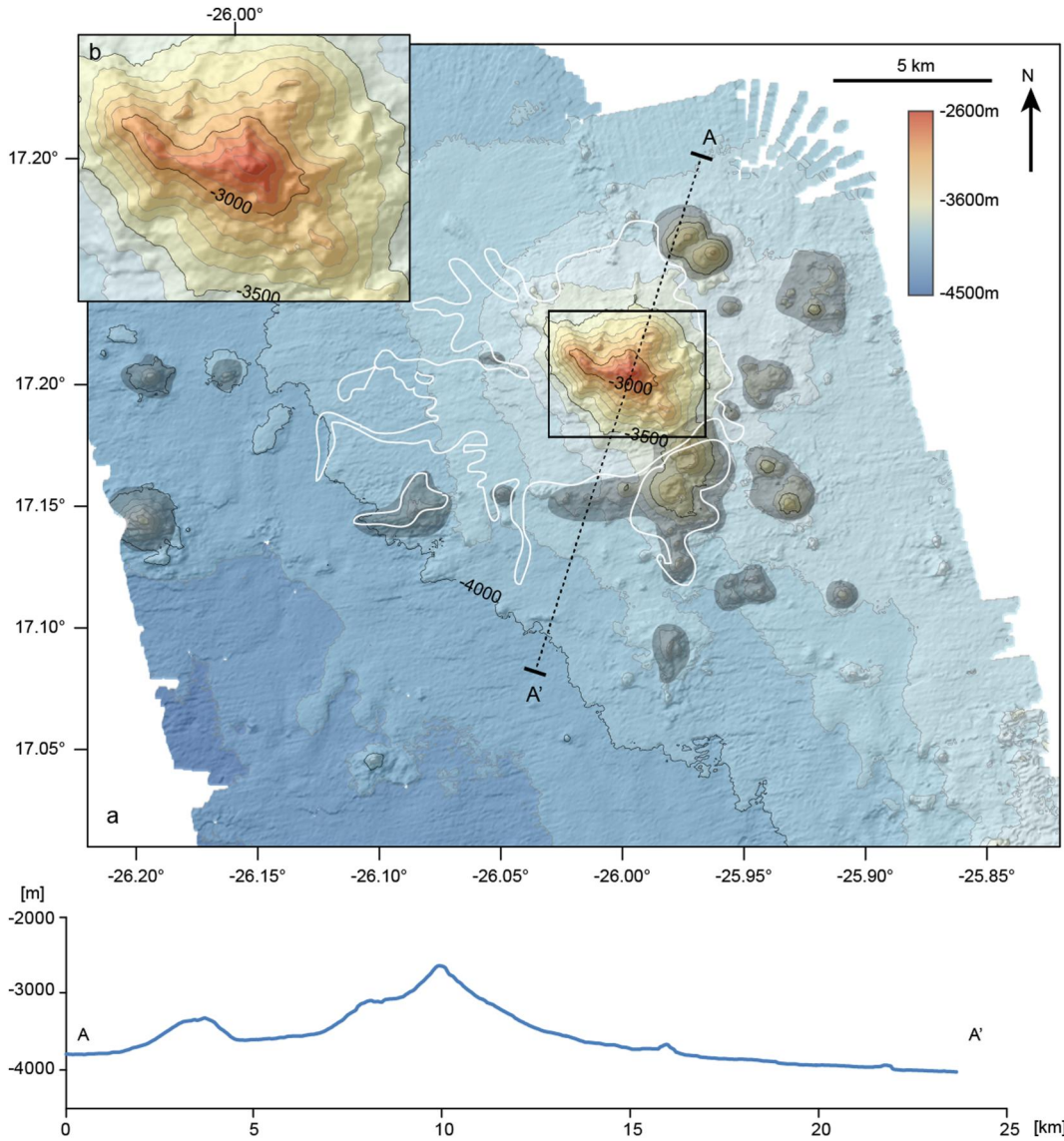

Figure 13. Geomorphological map of Sodade Seamount including 2x exaggerated cross section. White outlined area indicates high-backscatter areas (Figure S02.10 in Supporting Information S1).

Table 1
Summary Table of ^{40}Ar-^{39}Ar Analyses From Senghor Seamount

Material	Weighted mean age (2σ; Ma)	MSWD	*P* (%)	#	Inverse isochron age (95% conf.; Ma)	Initial $^{40}Ar/^{36}Ar$ (95% conf.)	MSWD	*P* (%)	SF (%)	#
Biotite	14.901 ± 0.034	0,67	93	#	14.911 ± 0.042	293.9 ± 4.1	0,67	92	57	#
K-feldspar	14.861 ± 0.029	1,15	25	#	14.841 ± 0.033	330 ± 28	0,99	48	7	#
	14.850 ± 0.029	0,55	98	#	14.845 ± 0.033	305 ± 31	0,55	97	5	#
	14.963 ± 0.051	0,31	91	6	14.927 ± 0.081	333 ± 66	0,01	100	5	6
K-feldspar and biotite	**14.872 ± 0.027**	1,02	42	#	14.867 ± 0.028	298.0 ± 3.2	1,01	46	60	#

Note. # = number of analyses, 95% conf. = 95% confidence, MSWD = Mean Squared Weighted Deviation, *P* = Probability, SF = Spreading Factor, and $^{40}Ar^*$ = radiogenic ^{40}Ar. Taylor Creek sanidine age = 28.344 ± 0.011 Ma (1σ; Fleck et al., 2019), and $^{40}K_{(total)} = 5.543\ (\pm 0.009) \times 10^{-10}$ years. Values in red indicate problematic values, for example, initial $^{40}Ar/^{36}Ar$ ratios >295.5, and low SF values (<40%). Age in bold indicates preferred age for sample.

yields an initial $^{40}Ar/^{36}Ar$ ratio of 330 ± 28 (95% conf.), which is higher than the atmospheric $^{40}Ar/^{36}Ar$ ratio of 295.5 (Steiger & Jäger, 1977), but the analyses are tightly clustered near the radiogenic ^{40}Ar axis (95%–100%), with a poor Spreading Factor value of 7%. We recommend the combined biotite and K-feldspar weighted mean ^{40}Ar-^{39}Ar age of 14.872 ± 0.027 Ma for the Senghor Seamount, which has never been geochronologically dated before (Table 1). This new ^{40}Ar-^{39}Ar age is the oldest seamount age for the Cabo Verde Archipelago and overlaps with K-Ar ages obtained from the southern islands chain and nearby islands of Sal and Maio (Mitchell et al., 1983; Torres et al., 2002).

6. Discussion

6.1. Location of Upper Pleistocene to Holocene Submarine Volcanic Activity

Our new seamount data demonstrate how Upper Pleistocene and younger igneous activity is distributed across considerable areas at both the NW and WSW tips of the respective northern and southern volcanic chains of the Cabo Verde Archipelago.

In the southern chain, not only are the islands of Fogo and Brava the sites of recent volcanic activity but also the seamounts Cadamosto and probably Tavares exhibit evidence for recent tectono-magmatic activity, as shown by shallow earthquakes and tremors spread out between Cadamosto and Brava island (Leva et al., 2020, 2022), and possibly also beneath Tavares (Faria & Fonseca, 2014). Brava island exhibits young (<262 ± 5 ka) onshore volcanic structures and sequences, including explosive activity during the last 250 kyrs (Madeira et al., 2010), and features an abundant record of volcano-tectonic earthquakes (Faria & Fonseca, 2014). The recent repeated eruptive activity of Fogo is also confirmed by a rich record of submarine tephra deposits resulting from large explosive eruptions near these two volcanoes (Eisele et al., 2015). Fogo on average produced one highly explosive eruption every 2000 years for the last 30 kyrs (Eisele et al., 2015) In agreement with our observations, Cadamosto Seamount is currently seismically active (Grevemeyer et al., 2009; Heleno et al., 2006; Helffrich et al., 2006; Leva et al., 2020, 2022), ^{40}Ar-^{39}Ar age data from Cadamosto lavas, showing eruption ages ranging from 97 ± 14 ka to as young as 21.40 ± 0.63 ka (Samrock et al., 2019), showing repeated late Quaternary activity. Likewise, Tavares Seamount, located further W of Brava and Cadamosto, exhibits a very clear volcanic edifice-construction morphology of a steep-sloped ridge, comparable to the pillow ridges of Sodade Seamount for which we have ROV evidence, completely devoid of pelagic/hemi-pelagic sediment cover, and was presumably also the site of Late Quaternary volcanism.

In the northern chain, Middle to Upper Pleistocene volcanic activity has previously been determined on the islands of São Nicolau (63.3 ± 45.3 and 57.1 ± 37.8 ka; Duprat et al., 2007), São Vicente (329 ± 60 ka; Holm et al., 2008) and Santo Antão (170 ± 20 and 90 ± 30 ka; Plesner et al., 2002). Our bathymetric and ROV observations suggest that the northern chain seamounts Sodade and the CDVF were also the sites of Upper Pleistocene or Holocene volcanic activity, based on the presence of very fresh sequences and recovered rock samples, young volcanic edifice-construction morphologies, and a thin pelagic/hemi-pelagic sediment cover. This is also supported by the high levels of seismicity in the area, with volcanic tremors being recorded at Santo Antão, CDVF and to a lesser extent, at Nola Seamounts, thus suggesting active volcanic processes are taking place at all these locations (Faria & Fonseca, 2014).

We therefore infer that active volcanism is occurring on the western termini of both the northern and southern chains in the Cabo Verde Archipelago. Our new seamount observations are consistent with modern seismic records and previous island studies. This suggests that Upper Pleistocene and Holocene volcanic activity is, as such, distributed over along-strike distances of 120 and 250 km in the southern and northern volcanic chains, respectively. The combined data show that young volcanic activity at Cabo Verde is: (a) more widespread than previously known and (b) also geographically distributed across several edifices with different ages and thus different evolutionary stages, which is consistent with the slow westward movement of the Cape Verde Plume relative to the African plate (Pollitz, 1991; Wang et al., 2018).

6.2. Evolutionary Stages of Cabo Verde Seamounts

The highly variable geomorphology of the Cabo Verde seamounts provides insights into the various stages of evolution of these submarine edifices and allows for correlation with the geological characteristics of the adjacent island edifices. Based on our observed geomorphological features, we have classified the Cabo Verde seamounts

according to three main stages of evolution: (a) an early growth stage (pre-shield and early shield), (b) a main growth stage (shield), and (c) erosion and rejuvenation stages. Details on the defining characteristics and respective interpretations are outlined below.

6.2.1. Early Growth Stage (Pre-Shield and Early Shield)

The volcanoes included in this initial stage are characterized by their small size and include both a main edifice (with or without smaller surrounding eruption centers), and semi-circular groups of small volcanoes with a combined extent of a few km. Volcanic fields covering several small volcanoes are included in this stage; however, satellite cones located on the flanks of a larger edifice are not included. Due to their limited size, these early growth volcanoes lack the following features: extensive or stellate rift zones, broad summit plateaus, large-scale mass-wasting scars, and spreading structures (caused by faulting; cf., Mitchell, 2001).

Starting at the NW end of the archipelago, SW of Santo Antão, the CDVF is interpreted to represent a young and still potentially active volcanic field, which is strongly supported by seismic data that suggests ongoing volcanism in this area (Faria & Fonseca, 2014). The CDVF comprises a number of individual and isolated small volcanoes, which resemble a small continental intraplate volcanic field (Figure 12). Judging by the relatively low volume of extruded volcanic rock compared to other structures discussed here, CDVF is interpreted to reflect an area of limited magmatic productivity, possibly representing a very early stage in seamount growth, before the amalgamation of several discrete volcanic centers into a more central volcanic system. The CDVF may thus herald the formation of a new, larger seamount, and thus represent an early pre-shield stage.

In the extreme NW of the archipelago, Sodade Seamount with its well exposed pillow ridges, steep slopes and still comparatively unfocused volcanic activity is considered an excellent example of a young submarine volcano in its early shield-building stage (Figure 13). Similar to CDVF, Sodade is the merely largest of a group of volcanic centers. The freshness of the pillow-lava sequences observed during ROV dives and from recovered samples, and the thin to absent sediment cover (Figures 2g and 2h) suggests that the seamount is active and growing at least in the Holocene. The edifice was also subjected to low-volume mass wasting (possibly syn-eruptive), a common process at this type of seamount that leads to the accumulation of loose pillow fragment breccias (talus) at the foot of small collapse scars, which contribute to the steepness of its flanks. Sodade may represent the type of edifice that the CDVF may ultimately evolve into, if the individual eruption centers become amalgamated. Many peripheral cones around Sodade indicate that the main volcano is just one of several centers of initial volcanism in this area. Thus, Sodade and its surrounding edifices may constitute a more advanced stage of a volcanic field similar to the characteristics described for the CDVF.

At the SW terminus of the archipelago, Tavares Seamount also appears to be comparatively young, exhibiting a clear, steep-sloped volcanic-construction morphology. Lava fields exposed nearby to the south support this view. This seamount is interpreted as a NNW-SSE-oriented sinuous volcanic ridge that, given its small size and lack of multiple rift zones/volcanic ridges, is considered to be in its early growth stage. However, this classification is provisional given the limited available data and lack of ROV observations.

6.2.2. Main Growth Stage (Shield)

Seamounts grow significantly in size through a combination of effusive and intrusive processes, resulting in more complex and mature magma plumbing systems. These seamounts typically include one or more main eruption centers or vent areas in their central regions. Satellite cones and well-preserved large collapse scars may be present but are not considered a defining feature. Shield-stage edifices may comprise well-defined rift zones radiating from the summit region, resulting in irregular or even stellate morphologies (Fornari et al., 1988; Mitchell, 2001; Schmidt & Schmincke, 2000; Walter et al., 2006). In some cases, edifices may also develop radial V-shaped extensional grabens that are genetically related to rift zones (e.g., the La Reunion Island; Delcamp et al., 2012). Edifices included in this stage are characterized by considerable volumes, a youthful volcanic morphology with a small, comparatively sharp summit, and may feature semi-radial rift zones (Fornari et al., 1988; Schmidt & Schmincke, 2000). On the basis of these characteristics, two Cabo Verde edifices fit these criteria—the Cadamosto and Maio Seamounts.

Maio Seamount (Figure 6) is a good example of a shield stage volcano featuring a large edifice (~2 km high) with a steep regular-slope volcanic growth morphology, including a rift zone and a summit crater that has partially

collapsed. The edifice exhibits a conspicuous NNE-SSW rift-graben system that is not filled by younger lavas, which is interpreted as a cessation of volcanic activity at the main growth stage. The absence of deep erosional gullies and significant mass-wasting structures such as upslope collapse scars, large-scale debris flow lobes, and downslope sediment wave fields suggests that this seamount had no post-erosional stage. The presence of only one satellite cone on its flanks also suggests that the edifice still exhibits a volcanic construction morphology resulting from a central feeding system and was not subjected to the widespread volcanism more typical of rejuvenated stages. The Maio Seamount is therefore interpreted to be a volcano that was arrested in its main (shield) building stage.

Cadamosto Seamount (Figure 9) has eruption ages of surface lavas ranging from at least 97 ± 14 to 21.40 ± 0.63 ky (Samrock et al., 2019), and stands almost 3 km above the surrounding seafloor. The seamount is the site of the highest seismic activity in the entire archipelago (Grevemeyer et al., 2009; Heleno et al., 2006; Helffrich et al., 2006), and exhibits clear signs of vigorous and ongoing volcano-seismic activity (Grevemeyer et al., 2009; Samrock et al., 2019), suggesting it is in the main shield-building stage. This is further supported by (a) the presence of at least four eruption centers in the summit region (Samrock et al., 2019), (b) the freshness of recovered rock samples, and (c) the absence of large erosional gullies on the volcano flanks. The upper slopes of the radial system of embayments and ridges show a number of smaller channels and gullies, whereas the lower two thirds of the slopes are very smooth, suggesting a comparatively high amount of mass wasting, and possibly the incipient development of rift zones. A significant area of the flanks has been mobilized due to mass wasting events (cf., Hansteen et al., 2014), which is a common feature in steep and rapidly growing submarine volcanoes subjected to seismic activity. The main edifice is dominated by phonolitic rocks (Barker et al., 2012; Samrock et al., 2019), which indicates the presence of crustal or uppermost mantle reservoirs where originally basaltic magmas went through extensive magmatic differentiation. Dominantly phonolitic islands and seamounts are unusual worldwide as high degrees of differentiation are required (e.g., Devey et al., 2003). Shallow intrusions of viscous phonolitic magmas beneath each of the four or more eruption centers may also have contributed to the observed higher degrees of mass wasting compared to other seamounts with less viscous mafic magma composition. The extrusion of evolved magmas may appear unusual for a volcanic seamount in its main building stage; however, the nearby volcanic edifice on Brava is also largely formed by phonolitic rocks (Madeira et al., 2010). We also interpret the large number of eruption centers between Cadamosto and Brava Island as a possible sign of future amalgamation between these two edifices or the formation of an additional seamount.

6.2.3. Post Shield, Erosional Stage and Rejuvenated Activity

As volcanoes mature and grow, shallower magma reservoirs form and intrusive rocks are emplaced at multiple levels below and within the volcanoes (cf., Mitchell, 2003), resulting in the formation of intrusive core complexes, which tend to induce lateral expansion of the edifices. The size of the edifices exerts major volcano-tectonic influences on the magma feeding system, and eruptive activity tends to spread toward the flanks, promoting the generation of satellite cones (see Gudmundsson et al., 2022). The formerly peaked summit areas broaden into plateaus with gentle slopes, with many of these plateaus having irregular to hummocky geomorphologies, attesting to constructive processes from more scattered volcanic centers (Schmidt & Schmincke, 2000). Seamounts with these characteristics are thus inferred to be in the late shield-building stage.

Once volcanic activity wanes, erosion, mass wasting, and gravitational spreading affect the edifices (e.g., Merle & Borgia, 1996). There may be a causal relationship between the amount of mass wasting, the degree of maturity and size of the volcanic edifice due to intrusive activity, including the formation of shallow magma chambers (e.g., Day et al., 1999; Mitchell, 2001). As a result, the edifices experience a slow degradation of their topography, acquiring distinctive geomorphological imprints such as erosional gullies, large collapse scars and associated debris flow lobes extending onto the surrounding seafloor, and extensional structures from the gravitational spreading of the weakened edifices (Klügel et al., 2005; Walter et al., 2006). Edifices with these traits may have entered the erosional stage of evolution.

Edifices in the rejuvenated (or post-erosional) stage are characterized by volcanism that post-dates the major erosional events. Typical features include eruption centers within landslide scars or covering previous tectonic or volcanic landforms. Pointed satellite cones and effusive structures are often superimposed on older edifice structures (Gudmundsson et al., 2022). Such presumably rejuvenated volcanism is frequent in the Cabo Verde Archipelago, with several islands (e.g., Santo Antão, Fogo) exhibiting more than one stage of post-erosional

eruptive activity, comprising sporadic and scattered volcanism of both mafic and intermediate/felsic compositions (Ancochea et al., 2012, 2014; Holm et al., 2008; Ramalho et al., 2010b; Ramalho, Helffrich, et al., 2010). By analogy, rejuvenated volcanism might also occur in the seamounts. However, without high-resolution bathymetric data from individual eruptive centers (e.g., satellite cones), widespread ROV observations or radiometric dating of recovered samples, the distinction between the erosion and rejuvenation stages in seamounts is complex and can be ambiguous.

Several seamounts show well-developed plateau morphologies, particularly the eastern seamounts of the southern chain (Senghor, Boavista, Cabo Verde, Maio Rise, and Tchadona), with the exception of Maio Seamount that has retained a cone shape with a summit peak and caldera indicative of the main growth (shield) stage. Cabo Verde Seamount comprises a fully developed submarine shield but never reached the subaerial stage as its summit plateau is still at a considerable depth (511 mbsl) and its hummocky terrain shows no signs of marine truncation or drowned coastlines. Nevertheless, there are signs of substantial erosion cutting into the presumed shield stage edifice. Boavista Seamount developed a hummocky summit plateau and, in contrast to Cabo Verde Seamount, accumulated substantial sedimentary cover. Maio Rise is more complex as it contains a smooth low-backscatter central plateau (Figure S2.5 in Supporting Information S1), which may be a sediment-filled depression surrounded by volcanic necks. Whether this summit was truncated by marine erosion is not clear; however, the shallow depth at which this summit occurs suggests this may be the case if some subsidence is considered. Tchadona Seamount shows similar features, with its shallow E plateau being truncated and sediment-covered, and the deeper W summit area showing hummocky terrain.

The Nola Seamounts have grown above sea level and formed islands, which influenced their summit morphologies (see Chapter 6.2.4). At the same time, the flanks of these two seamounts are comparatively undisturbed by erosion (Masson et al., 2008). A particular characteristic of Nola, and the undisturbed flanks of the other eastern Cabo Verde seamounts (except Maio) is the profuse occurrence of satellite eruption centers, which probably would not be preserved if the slopes had been mobilized. Therefore, we assume that the Nola Seamounts are either in an erosional or even a rejuvenated stage.

Among the investigated seamounts, Senghor (Figure 3) displays the most prominent fault system, although faults are also evident on Cabo Verde and Boavista (Figures 4 and 5). Senghor does not display large landslide scars but does feature a complicated structure of arcane grabens in the SW sector (Figure 3). Similar but less well-developed features are found at Cabo Verde and Boavista, and perhaps Nola West (Figures 4, 5, and 11), which are interpreted as extensional structures formed by gravitational spreading (Walter et al., 2006). The volcanic evolution of Maio Rise and Boavista Seamount appears to have halted at a similar stage. Mass wasting and gravitational spreading have reduced particularly the latter to a skeletal shape similar to the stellate shape of El Hierro in the Canary Islands (Carracedo, 1999).

In summary, the seamounts of Senghor, Boavista, Cabo Verde, Maio Rise, Tchadona and the Nolas are considered to be in their erosional/rejuvenated stages. This interpretation relies on their similar erosional features and possible late-stage volcanism. More detailed work on their satellite cones, which timing we can only attribute based on aforementioned generalized concepts of island evolution, will allow us to establish if post-erosional volcanism did indeed occur in these edifices, and consequently if these edifices are either in their erosion or rejuvenation stages.

6.2.4. Evidence for Emergence and Coastal Erosion

The flat summit-plateaus on Senghor, Nola, and Tchadona seamounts indicate that these volcanic edifices are guyots—former islands truncated by erosion. We infer those features, as well as additional former coastal terraces in even lower positions, from the bathymetrical maps (Figure 14), but especially from carefully chosen profiles of this bathymetry (Figure 15). For Senghor, the relief across the 7.9 km^2 plateau area is ~40 m. Similar estimates for Nola West and Nola East yield areas and relief values of 6.6 km^2 and 100 m and 6.7 km^2 and 65 m, respectively. Tchadona has a summit-plateau area of 22 km^2 and a relief of 120 m. The edges of the summit-plateau are defined at −160 mbsl for these seamounts, which is where the slope becomes ubiquitously steep at all seamounts. The observed flat and regular summit-plateaus on these seamounts are interpreted as formerly exposed shorelines, for example, marine-erosion plateaus, subsequently drowned by isostatic movement due to subsidence and/or a glacio-eustatic sea level rise of up to 120 m since the Last Glacial Maximum at 26–20 ka (Waelbroeck et al., 2002). Their edges are frequently abrupt, suggesting truncation by wave erosion, forming now-submerged

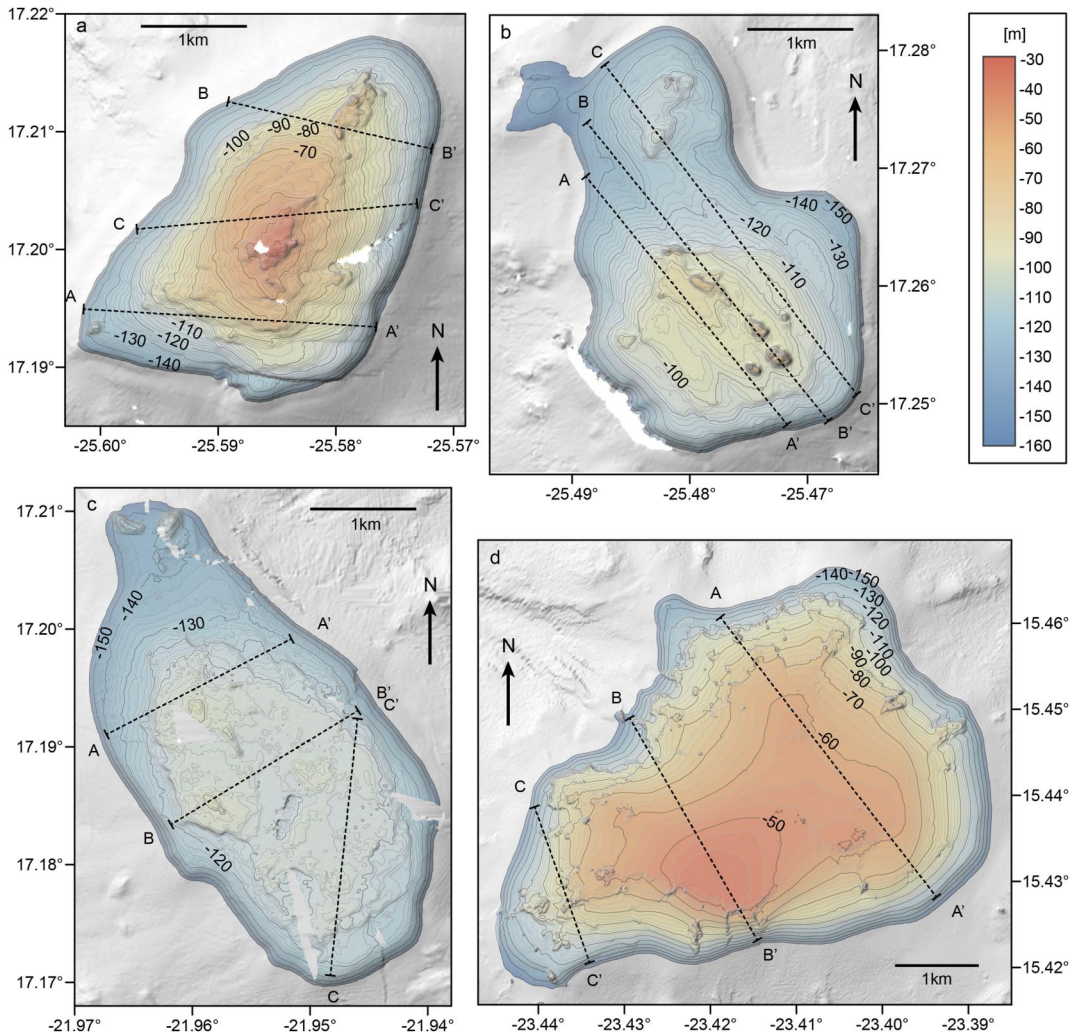

Figure 14. Bathymetrical maps of the summit plateaus of (a) Nola West, (b) Nola East, (c) Senghor, and (d) Tchadona seamounts. Depth contours were drawn down to 160 m, below which only shaded relief is shown. Marked cross-sections refer to Figure 15.

sea cliffs. Comparing the relief undulation, summit-plateaus at Senghor and Tchadona are more eroded than those at the Nolas, which may suggest that Senghor and Tchadona are older and the Nolas are younger. Although these seamounts have a comparable amount of undulation in their relief, a domed edifice tops the plateau on Nola West, while Nola East still shows a number of residual volcanic necks (Figure 15) that may either point to a comparatively compact volcanic edifice or to comparatively less amount of wave cut erosion.

Correlating between the present positions of drowned-coastal summit-plateaus and lower coastal-terraces versus eustatic sea level curves (e.g., Miller et al., 2011) can provide insights into isostatic movements affecting volcanic edifices. The 14.9 Ma Senghor and younger Nola seamounts show evidence of emergences above sea level in the form of several drowned summit-plateaus and coastal-terraces visible as a step-wise morphology in the profiles (Figure 15). Senghor has a summit-plateau and coastal-terraces at depths of −106, −120, and −128 m, and a summit-plateau and coastal-terraces are found at −67, −85, −98, −106, −129, and −230 m depths on Nola West, and −71, −96, −110, −116, and −260 m depths on Nola East. Some of the summit-plateaus and coastal-terraces of Nola East and West may represent the same events (e.g., −71 and −67 m summit-plateaus and −98 and −96 m coastal-terraces, respectively) with minor differences due to local volcano-tectonic activity or different responses to wave erosion owing to varying lithological properties. Tchadona Seamount has a somewhat rounded summit plateau at ~40–60 m depth, and individual coastal-terraces at −80, −93, −115, −120, and eventually also at −141 m depths. The majority of these drowned marine terraces are within the range of the eustatic amplitude

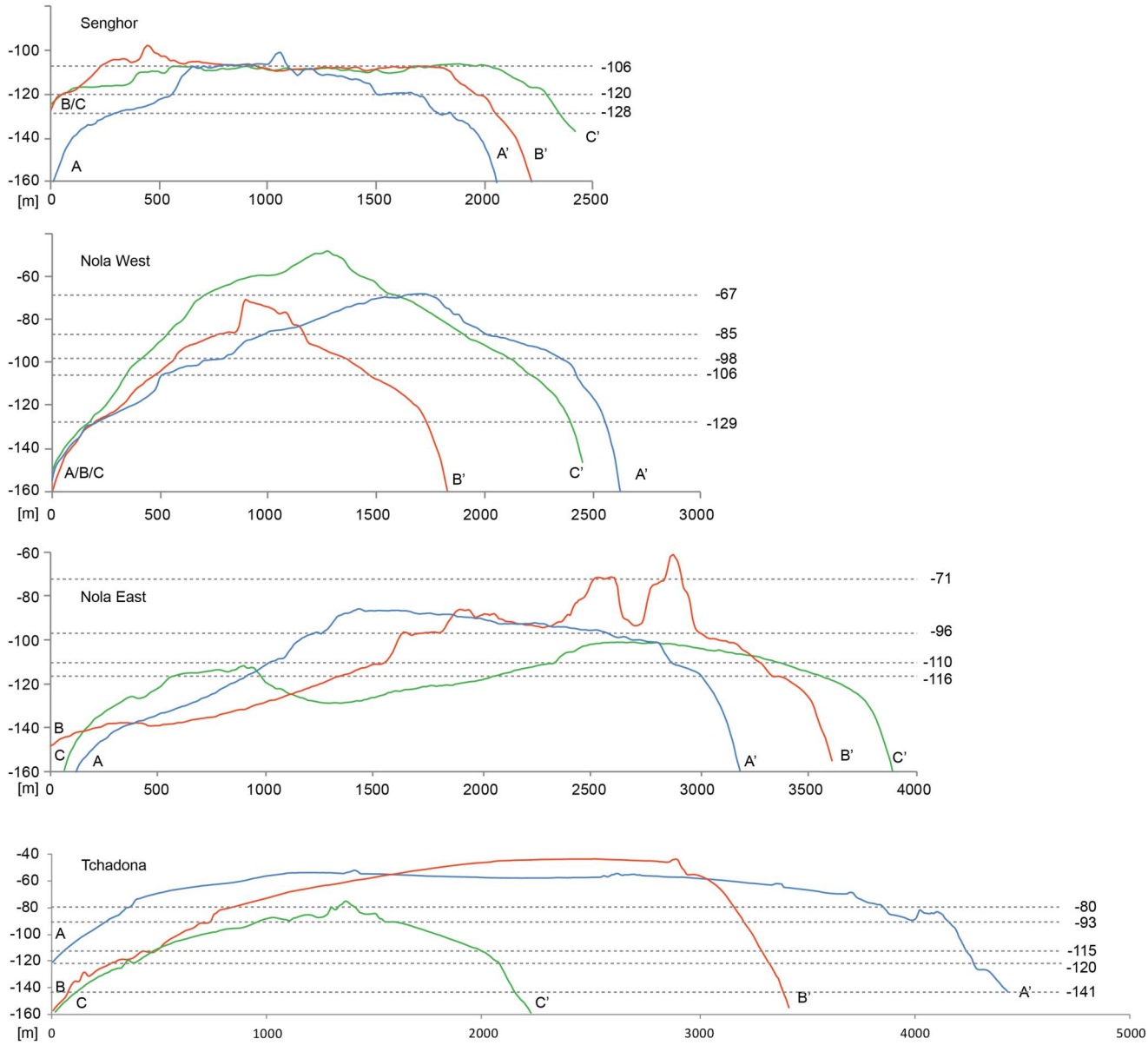

Figure 15. Stacked cross-sections of the Senghor, Nolas and Tchadona seamounts are shown in Figure 14, with 10x vertical exaggeration. Dashed lines and values on the right indicate the vertical positions of drowned marine terraces (wave cut surfaces).

(−120 to +50 m; Miller et al., 2011) over the whole 26 Ma volcanic history of the Cabo Verde Archipelago, but due to the lack of absolute ages of these terraces and their sedimentary deposits, no precise isostatic movements can be inferred.

Senghor Seamount exhibits some drowned marine terraces that are shallower than the −120 m eustatic sea-level minima as a result of the Last Glacial Maxima at 26–20 ka (Miller et al., 2011), which suggests that either this seamount did not experience any subsidence, or the subsidence was compensated by more recent uplift. Moreover, the razed and leveled summit-plateau at Senghor suggests sustained erosion during several eustatic cycles, resulting in its complete truncation. This is consistent with the 14.9 Ma age obtained from this edifice, providing ample time of several glacial cycles for such a complete abrasion of the summit. Additionally, the lower marine terraces at Senghor (−128 and −120 m) are similar to the −120 m depth of the Last Glacial Maximum sea-level lowstand; therefore, these marine terraces may have eroded during this 26-20 ka event (Miller et al., 2011). Possible earlier events forming the shallower marine terraces are more difficult to constrain, as the glacio-eustatic

sea level cycles drive the sea level rise and fall across these coastal marks comparatively often (Miller et al., 2011). In this respect, the large shallow platform of the Maio-Boa Vista basements, to be studied in the future, may provide better constraints as they show less vertical movement due to their greater age than Senghor, and especially less compared to the Nola Seamounts.

The lowest terraces at the Nola East (−230 m) and Nola West (−260 m) seamounts (Figures 11, 14, and 15) are deeper than the eustatic minima of −120 m (Miller et al., 2011). We interpret these deeper marine terraces as old, drowned shorelines, which may have subsequently experienced subsidence. This subsidence may be due to surface loading from the recent volcanic growth of Santo Antão Island, which is in agreement with onshore studies by Ramalho et al. (2010b). Note that the Nola Seamounts lap onto Santo Antão, which is morphologically older. Tchadona seamount also exhibits a terrace just slightly below the eustatic minima, but given the proximity between these levels (−141 and −130 m), no significant net subsidence is inferred for this seamount.

The rates of vertical movement have previously been constrained on the Cabo Verde islands (Ramalho et al., 2010a, 2010b; Ramalho, Helffrich, et al., 2010), and uplift of almost the entire archipelago by 100 m during the Quaternary period has occurred due to inflation of the Cabo Verde Rise. This should be taken into account in future detailed investigations of coastline reconstructions. Notwithstanding this regional uplift signal, observations onshore suggest a complex long-term uplift/subsidence history for the Cabo Verde islands, even if they are subjected to net uplift trends, as it happens with Santiago, São Nicolau, and Brava (Ramalho, 2011; Ramalho et al., 2010a, 2010b; Ramalho, Helffrich, et al., 2010; Madeira et al., 2010; Marques et al., 2020). Moreover, individual islands exhibit different uplift/subsidence histories, demonstrating that isostatic movements are dominated by local processes (such as jacking by intrusive activity at the base of the edifices—see Carvalho et al., 2022) that operate at different times and spatial scales at each individual island (Ramalho et al., 2010a, 2010b; Ramalho, Helffrich, et al., 2010). This means that without detailed geochronology for the seamount sequences and their relative sea-level markers, correlating isostatic movements on individual seamounts with neighboring islands is not possible, or is extremely complex and speculative.

In summary, the truncated summit-plateaus and lower submerged marine terraces found on the respective top and flanks of several seamounts (Senghor, Tchadona and the Nolas) demonstrate that these edifices are guyots. Moreover, given that several of these seamounts have summits above the eustatic minima for the last 26 Ma, these edifices may have been islands (i.e., were above sea level) during sea-level lowstands. If so, the emerged area of the archipelago during these lowstands was significantly larger, which has important implications for paleogeographical reconstructions of the archipelago, for example, in biogeographical studies (e.g., Ávila et al., 2019).

6.3. Morphological Evolution of the Cabo Verde Archipelago

Using the combined subaerial and submarine geomorphology of the Cabo Verde Archipelago, we can identify three main platforms connecting these groups of islands, and additional solitary seamounts in the east (Senghor, Boavista, Cabo Verde and Maio seamounts; Figures 1 and 16). The East Platform (EP) comprises the islands of Sal, Boa Vista, Maio and Santiago, as well as João Valente Bank and Tchadona Seamount. These edifices are separated by water depths of 1,000 m or less. The geomorphological relief is particularly broad and shallow between the more eroded islands from Sal to Maio, attesting to their advanced developmental stages. The João Valente Bank rises to locally only 14 m beneath sea level (Ramalho, 2011), forming a flat top summit area at 80–100 mbsl comparable to the size of the nearby islands. It may constitute a drowned island in its guyot stage similar to the nearby Tchadona Seamount. The Northwest Platform (NWP) comprises the islands of São Nicolau, Raso, Branco, Santa Luzia, São Vicente and Santo Antão, and the flat-topped Nola Seamounts. The islands of Fogo and Brava, with the addition of Cadamosto Seamount and Ilhéus Secos form the Southwest Platform (SWP). The NWP and EP are separated by ∼90 km, while the SWP and EP are ∼30 km apart.

Maio Rise and the Boavista and Tchadona seamounts are located on the lower flanks of the EP. The active Cadamosto Seamount shows a morphological link to Brava in the SWP. Similarly, the Nola seamounts and the CDVF are located offshore from Santo Antão island, with the former located along the axis of the NWP, and the latter perpendicular to the NWP. Both the SWP and NWP have a western continuation through the morphologically young Sodade and Tavares seamounts, respectively.

Considering the radiometric ages of the Cabo Verde islands and seamounts, the occurrence of three separate platforms has geodynamic implications. The EP is the oldest platform, and its construction was probably initiated

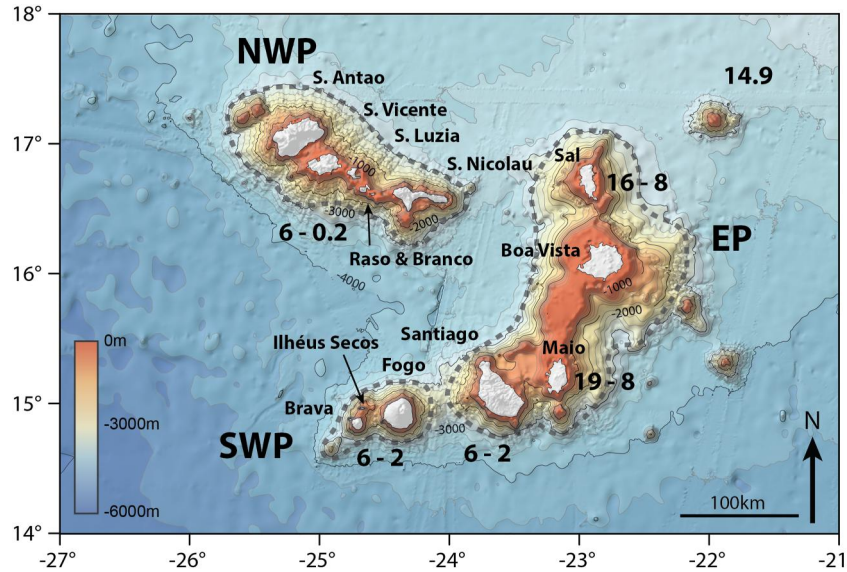

Figure 16. Global Multi-Resolution Topography map (Ryan et al., 2009) of the Cabo Verde Archipelago. Islands are colored white. The platforms East (EP), Southwest (SWP) and Northwest (NWP) and the age ranges of their shield stages are shown (dashed lines). Also included is the new ^{40}Ar-^{39}Ar age for Senghor Seamount (boldface numbers in Ma). Other ages are based on data from Ancochea et al. (2010, 2012, 2014, 2015), Bernard-Griffiths et al. (1975), Duprat et al. (2007), Dyhr and Holm (2010), Foeken et al. (2009), Grunau et al. (1975), Holm et al. (2008), Madeira et al. (2005, 2010), Mitchell et al. (1983), Plesner et al. (2002), and Torres et al. (2002).

in the Late Oligocene—Early Miocene, with construction beginning in the eastern portion. The shield stage ages of 26 to 9 Ma in the EP are comparable to the 14.9 Ma age of Senghor Seamount (ages compiled in Samrock et al., 2019) (Figure 16). However, judging from the island ages, the growth of the westernmost edifice on Santiago Island in the EP was contemporaneous with the construction of the NWP and SWP during the Upper Miocene and Pliocene (Holm et al., 2008; Ramalho, 2011), with an age overlap between 8 and 6 Ma. The break in geomorphology west of the EP means that there was a "jump" in the location of igneous activity, and simultaneously a change in the geometry of the archipelago. Evidence is thus given both by overlapping radiometric ages between islands on the three platforms and by their physical separation. This represents the westward migration of active volcanism to both the SWP and the western sector of the NWP, whilst more sporadic post-erosional low-volume volcanism continued to take place along the EP and the eastern sector of the NWP. The newly discovered Tavares and Sodade seamounts thus represent the western continuations of the active SWP and NWP platforms, respectively. Due to their locations on the west edges of the platforms, they are interpreted to represent comparatively young features, heralding the shift of volcanic activity even further westwards.

6.4. Deep-Water Explosive Volcanism at CDVF

In the CDVF, the craters of Tambor and Kolá are wide and comparatively shallow, exhibit nearly vertical walls with well-exposed pyroclastic sequences, and are characterized by flat crater floors. Kolá is a morphological depression ∼1 km wide within a group of smaller volcanic cones. These features closely resemble subaerial or shallow-water tuff rings. Such characteristics, including the presence of fresh mafic pyroclastic sequences and deposits in clear genetic relationship with these craters, are suggestive of highly fragmenting explosive eruption mechanisms, despite the great depth at which these cones rest. Deep-water explosive volcanism is rare worldwide, particularly at depths below the critical point for seawater (3,000 m; Sohn et al., 2008; White et al., 2003) and yet the CDVF exhibits several structures that clearly attest to the occurrence of such phenomena. Future studies on the samples collected from these sites, as well as the analysis of the sequences observed, will shed light on the origin of these eruptions, but a mechanism involving the eruption of magmas extremely rich in volatiles (particularly CO_2) is tentatively suggested as the most probable reason to explain the high volcanic fragmentation at these depths. This hypothesis is supported by the occurrence of unusually high CO_2 contents in primitive magmas from Fogo volcano, interpreted to drive their ascent and explosivity (DeVitre et al., 2023).

7. Conclusions

We have presented the first combined comprehensive geomorphological study and interpretation of Cabo Verde seamounts and incipient submarine volcanic edifices based on multibeam bathymetry data and seafloor observations by ROV. Taken together, the seamount and island data suggest a shift in igneous activity from the EP to both the NWP and SWP platforms at about 8–6 Ma. Overlapping radiometric ages across and within the platforms suggest that at any time during evolution of the archipelago, volcanism was spread out across distances of about 100–150 km. The continuing westward extent of the NWP and SWP has been expanded by the discovery of the previously unknown Sodade and Tavares seamounts. The state of preservation of these seamounts generally matches the observed westward age progression of volcanism along the two island chains. We report evidence of particularly deep explosive volcanic activity around 4,000 mbsl at the CDVF, which may be related to unusually high CO_2 contents of the magmas. Our new ^{40}Ar-^{39}Ar age of Senghor Seamount and inferred/recent volcanic activity of the other seamounts reveal that within a distance of ∼100 km on each end of the northern and southern chains, the propagation of volcanism is clear, albeit diffusely oriented. A key conclusion of our study is that the general westward migration of volcanic activity is reflected in the volcanic edifices morphological state of maturity in both the Cabo Verde islands and seamounts. This suggests the progressive westward migration of the Cabo Verde plume or more likely the eastward movement of the Nubia plate over the Cabo Verde hot spot.

Pleistocene emergence and marine erosion are suggested for the summits of the Nola and Senghor seamounts, which feature drowned marine terraces, and the observed ∼120 m coastal terraces may correspond to the sea-level lowstands of the Last Glacial Maximum at 26–20 ka. This implies that the Nola Seamounts are a comparatively young feature in the NW Cabo Verde, where rejuvenated volcanic activity predates the Last Glacial Maximum.

Data Availability Statement

Adhering to the FAIR principles of data sharing, the data used in this publication is openly available as follows: The multibeam swath echo sounder data of the RV METEOR cruises referenced in this publication are available through the Pangea Repository at https://doi.pangaea.de/10.1594/PANGAEA.935344 for M80/3 (Hansteen et al., 2021) https://doi.pangaea.de/10.1594/PANGAEA.923998 for M79/3 (Christiansen & Wölfl, 2020) https://doi.pangaea.de/10.1594/PANGAEA.960035 for M62/3 (Grevemeyer, 2023). The CD168 data are referenced in Masson et al., 2008 and through the cruise report available at https://www.bodc.ac.uk/resources/inventories/cruise_inventory/report/6749/. The Tchadona Seamount bathymetry was not collected during a dedicated scientific cruise but is available through a dedicated repository of the Portuguese Hydrographic Institute: https://gridmarcv.hidrografico.pt/. In addition, it is available at (Leitão et al., 2024). The data of the Ar-Ar age dating analyses are available at (Wartho et al., 2024).

Acknowledgments
We appreciate the support of the government of the Republic of Cabo Verde for providing permission to work in their territorial waters. We thank B. Christiansen and the party of cruise M79/3 for the opportunity to collect additional multibeam data and dredge samples. The METEOR expedition 80/3 was funded by the Deutsche Forschungsgemeinschaft (DFG, German Research Council) and the Bundesministerium für Bildung, Wissenschaft, Forschung und Technologie (BMBF, Federal Ministry of Education and Research). We express our gratefulness to Captain Wunderlich and his crew for their professionality. We further acknowledge the invaluable support of the GEOMAR ROV team. We thank Capt. João Paulo Delgado Vicente of the Instituto Hidrográfico, Lisboa, Portugal, for the permission to use the digital base map of the Tchdona Seamount as part of a data exchange agreement. Jan Sticklus is thanked for his invaluable laboratory support with ^{40}Ar-^{39}Ar dating of the Senghor Seamount sample. T. Kwasnitschka acknowledges financial support through the Jeddah Transect Project and the Helmholtz Alliance ROBEX. R.S. Ramalho ackowledges his IF/01641/2015 contract as well as support from PTDC/CTA-GEO/28588/2017 and LISBOA-01-0145-FEDER-028588 project UNTIeD, co-funded by the European Regional Development Fund—ERDF, through Programa Operacional Regional de Lisboa (POR Lisboa 2020), and by FCT—Fundação para a Ciência e a Tecnologia I.P. Open Access funding enabled and organized by Projekt DEAL.

References

Ali, M. Y., Watts, A. B., & Hill, I. (2003). A seismic reflection profile study of lithospheric flexure in the vicinity of the Cabo Verde Islands. *Journal of Geophysical Research*, *108*(B5), 2239. https://doi.org/10.1029/2002JB002155

Ancochea, E., Hernán, F., Huertas, M. J., & Brändle, J. L. (2012). A basic radial dike swarm of Boa Vista (Cabo Verde Archipelago); its significance in the evolution of the island. *Journal of Volcanology and Geothermal Research*, *243*, 24–37. https://doi.org/10.1016/j.jvolgeores.2012.06.029

Ancochea, E., Huertas, M. J., Hernán, F., & Brändle, J. L. (2010). Volcanic evolution of São Vicente, Cabo Verde Islands: The Praia Grande landslide. *Journal of Volcanology and Geothermal Research*, *198*(1), 143–157. https://doi.org/10.1016/j.jvolgeores.2010.08.016

Ancochea, E., Huertas, M. J., Hernán, F., & Brändle, J. L. (2014). A new felsic cone-sheet swarm in the Central Atlantic Islands: The cone-sheet swarm of Boa Vista (Cabo Verde). *Journal of Volcanology and Geothermal Research*, *274*, 1–15. https://doi.org/10.1016/j.jvolgeores.2014.01.010

Ancochea, E., Huertas, M. J., Hernán, F., Brändle, J. L., & Alonso, M. (2015). Structure, composition and age of the small islands of Santa Luzia, Branco and Raso (Cape Verde Archipelago). *Journal of Volcanology and Geothermal Research*, *302*, 257–272. https://doi.org/10.1016/j.jvolgeores.2015.07.015

Ávila, S. P., Melo, C., Berning, B., Sá, N., Quartau, R., Rijsdijk, K. F., et al. (2019). Towards a 'Sea-Level Sensitive' dynamic model: Impact of island ontogeny and glacio-eustasy on global patterns of marine island biogeography. *Biological Reviews*, *94*(3), 1116–1142. https://doi.org/10.1111/brv.12492

Barker, A. K., Hansteen, T. H., & Nilsson, D. (2019). Unravelling the crustal architecture of Cape Verde from the seamount xenolith record. *Minerals*, *9*(90), 1–13. https://doi.org/10.3390/min9020090

Barker, A. K., Holm, P. M., Peate, D. W., & Baker, J. A. (2010). A 5 million year record of compositional variations in mantle sources to magmatism on Santiago, southern Cape Verde archipelago. *Contributions to Mineralogy and Petrology*, *160*(1), 133–154. https://doi.org/10.1007/s00410-009-0470-x

Barker, A. K., Troll, V. R., Ellam, R. M., Hansteen, T. H., Harris, C., Stillman, C. J., & Andersson, A. (2012). Magmatic evolution of the Cadamosto Seamount, Cabo Verde: Beyond the spatial extent of EM1. *Contributions to Mineralogy and Petrology*, *163*(6), 949–965. https://doi.org/10.1007/s00410-011-0708-2

Barrett, R., Lebas, E., Ramalho, R., Klaucke, I., Kutterolf, S., Klügel, A., et al. (2020). Revisiting the tsunamigenic volcanic flank-collapse of Fogo Island in the Cabo Verdes, offshore West Africa. *Geological Society of London, Special Publications*, *500*(1), 13–26. https://doi.org/10.1144/SP500-2019-18

Bernard-Griffiths, J., Cantagrel, J.-M., Matos Alves, C. A. A., Mendes, F., Serralheiro, A., & Rocha de Macedo, J. (1975). Données radiométriques potassium-argon sur quelques formations magmatiques des iles de l'archipel du Cap Vert. In G. Villards (Ed.), *Comptes Rendus Hebdomadaires Des Séances de l'Académie Des Sciences, Série D: Sciences Naturelles 03* (pp. 2429–2432). Gauthier-Villars.

Burke, K., & Wilson, J. T. (1972). Is the African plate stationary? *Nature*, *239*(5372), 387–390. https://doi.org/10.1038/239387b0

Carracedo, J. C. (1999). Growth, structure, instability and collapse of Canarian volcanoes and comparisons with Hawaiian volcanoes. *Journal of Volcanology and Geothermal Research*, *94*(1), 1–19. https://doi.org/10.1016/S0377-0273(99)00095-5

Carvalho, J., Bonadio, R., Silveira, G., Lebedev, S., Mata, J., Arroucau, P., et al. (2019). Evidence for high temperature in the upper mantle beneath Cabo Verde Archipelago from Rayleigh-wave phase-velocity measurements. *Tectonophysics*, *770*, 228225. https://doi.org/10.1016/j.tecto.2019.228225

Carvalho, J., Silveira, G., Dumont, S., & Ramalho, R. (2022). 3D-ambient noise surface wave tomography of Fogo volcano, Cape Verde. *Journal of Volcanology and Geothermal Research*, *432*, 107702. https://doi.org/10.1016/j.jvolgeores.2022.107702

Christiansen, B., Brand, T., Büntzow, M., Busecke, J., Coelho, R., Correia, S., et al. (2011). *Structure and function of seamount ecosystems in the Cape Verde Region, Northeast Atlantic - Cruise No. 79/3 - September 24–October 23, 2009 - Las Palmas/Spain - Mindelo/Cape Verde* (pp. 1–53). DFG-Senatskommission für Ozeanographie. https://doi.org/10.2312/cr_m79_3

Christiansen, B., & Wölfl, A.-C. (2020). Multibeam bathymetry raw data (Kongsberg EM 120 entire dataset) of RV METEOR during cruise M79/3 [Dataset]. *PANGAEA*. https://doi.org/10.1594/PANGAEA.923998

Clague, D. A., & Dalrymple, G. B. (1987). The Hawaiian-Emperor volcanic chain. Part I. Geologic evolution. In R. W. Decker, T. L. Wright, & P. H. Stauffer (Eds.), *Volcanism in Hawaii*, *U.S. Geological Survey Professional Paper 1350* (Vol. 1, pp. 5–54).

Clemmensen, L. B., & Holm, P. M. (2020). Ash-bearing transgressive coastal dune on São Vincente (Cape Verde Islands): Dune history and evidence of explosive volcanic activity around 35 ka. *International Journal of Earth Sciences*, *109*(1), 159–170. https://doi.org/10.1007/s00531-019-01795-7

Courtney, R. C., & White, R. S. (1986). Anomalous heat flow and geoid across the Cabo Verde Rise: Evidence for dynamic support from a thermal plume in the mantle. *Geophysical Journal International*, *87*(3), 815–867. https://doi.org/10.1111/j.1365-246X.1986.tb01973.x

Davies, G. F. (1988). Ocean bathymetry and mantle convection 1. Large-scale flow and hotspots. *Journal of Geophysical Research*, *93*(9), 10467–10480. https://doi.org/10.1029/JB093iB09p10467

Day, S., Heleno da Silva, S. I. N., & Fonseca, J. F. B. D. (1999). A past giant lateral collapse and present-day flank instability of Fogo, Cabo Verde Islands. *Journal of Volcanology and Geothermal Research*, *94*(1–4), 191–218. https://doi.org/10.1016/S0377-0273(99)00103-1

Delcamp, A., de Vries, B. V. W., James, M. R., Gailler, L. S., & Lebas, E. (2012). Relationships between volcano gravitational spreading and magma intrusion. *Bulletin of Volcanology*, *74*(3), 743–765. https://doi.org/10.1007/s00445-011-0558-9

Devey, C. W., Lackschewitz, K. S., Mertz, D. F., Bourdon, B., Cheminée, J.-L., Dubois, J., et al. (2003). Giving birth to hotspot volcanoes: Distribution and composition of young seamounts from the seafloor near Tahiti and Pitcairn islands. *Geology*, *31*(5), 395–398. https://doi.org/10.1130/0091-7613(2003)031<0395:GBTHVD>2.0.CO;2

DeVitre, C. L., Gazel, E., Ramalho, R. S., Venugopal, S., Steele-MacInnis, M., Hua, J., et al. (2023). Oceanic intraplate explosive eruptions fed directly from the mantle. *Proceedings of the National Academy of Sciences*, *120*(33), e2302093120. https://doi.org/10.1073/pnas.2302093120

Doucelance, R., Escrig, S., Moreira, M., Gariepy, C. M., & Kurz, M. (2003). Pb-Sr-He isotope and trace element geochemistry of the Cabo Verde Archipelago. *Geochimica et Cosmochimica Acta*, *67*(19), 3717–3733. https://doi.org/10.1016/S0016-7037(03)00161-3

Duprat, H. I., Friis, J., Holm, P. M., Grandvuinet, T., & Sorensen, R. V. (2007). The volcanic and geochemical development of Sao Nicolau, Cabo Verde Islands: Constraints from field and $^{40}Ar/^{39}Ar$ evidence. *Journal of Volcanology and Geothermal Research*, *162*(1–2), 1–19. https://doi.org/10.1016/j.jvolgeores.2007.01.001

Dyhr, C. T., & Holm, P. M. (2010). A volcanological and geochemical investigation of Boa Vista, Cape Verde Islands; $^{40}Ar/^{39}Ar$ geochronology and field constraints. *Journal of Volcanology and Geothermal Research*, *189*(1–2), 19–32. https://doi.org/10.1016/j.jvolgeores.2009.10.010

Eisele, S., Reißig, S., Freundt, A., Kutterolf, S., Nürnberg, D., Wang, K. L., & Kwasnitschka, T. (2015). Pleistocene to Holocene offshore tephrostratigraphy of highly explosive eruptions from the southwestern Cabo Verde Archipelago. *Marine Geology*, *369*, 233–250. https://doi.org/10.1016/j.margeo.2015.09.006

Faria, B., & Fonseca, J. F. B. D. (2014). Investigating volcanic hazard in Cabo Verde Islands through geophysical monitoring: Network description and first results. *Natural Hazards and Earth System Sciences*, *14*(2), 485–499. https://doi.org/10.5194/nhess-14-485-2014

Faugeres, J. C., Legigan, P., Maillet, N., & Latouche, C. (1986). Pelagic, turbiditic, and contouritic sequential deposits on the Cabo Verde Plateau (Leg 108, Site 659, Northwest Africa): Sediment record during Neogene time. In *Proceedings of the Ocean Drilling Program: Scientific results* (Vol. 108, pp. 311–327).

Fleck, R. J., Calvert, A. T., Coble, M. A., Wooden, J. L., Hodges, K., Hayden, L. A., et al. (2019). Characterization of the rhyolite of Bodie Hills and $^{40}Ar/^{39}Ar$ intercalibration with Ar mineral standards. *Chemical Geology*, *525*, 282–302. https://doi.org/10.1016/j.chemgeo.2019.07.022

Foeken, J. P. T., Day, S. J., & Stuart, F. M. (2009). Cosmogenic ^{3}He exposure dating of the Quaternary basalts from Fogo, Cape Verdes: Implications for rift zone and magmatic reorganisation. *Quaternary Geochronology*, *4*(1), 37–49. https://doi.org/10.1016/j.quageo.2008.07.002

Fornari, D. J., Garcia, M. O., Tyce, R. C., & Gallo, D. G. (1988). Morphology and structure of Loihi seamount based on seabeam sonar mapping. *Journal of Geophysical Research*, *93*(B12), 15227–15238. https://doi.org/10.1029/JB093iB12p15227

Freitas, R., Falcón, J. M., González, J. A., Burnett, K. A., Dureuil, M., Caruso, J. H., et al. (2018). New and confirmed records of fishes from the Cabo Verde Archipelago based on photographic and genetic data. *Arquipelago. Life and Marine Sciences*, *35*, 67–83.

Geldmacher, J., Hoernle, K., van den Bogaard, P., Duggen, S., & Werner, R. (2005). New $^{40}Ar/^{39}Ar$ age and geochemical data from seamounts in the Canary and Madeira volcanic provinces: Support for the mantle plume hypothesis. *Earth and Planetary Science Letters*, *237*(1), 85–101. https://doi.org/10.1016/j.epsl.2005.04.037

Geldmacher, J., Hoernle, K., van den Bogaard, P., Zankl, G., & Garbe-Schönberg, D. (2001). Earlier history of the ≥70-Ma-old Canary hotspot based on the temporal and geochemical evolution of the Selvagen Archipelago and neighboring seamounts in the eastern North Atlantic. *Journal of Volcanology and Geothermal Research*, *111*(1–4), 55–87. https://doi.org/10.1016/S0377-0273(01)00220-7

Gerlach, D. C., Cliff, R. A., Davies, G. R., Norry, M., & Hodgson, N. (1988). Magma sources of the Cape-Verdes archipelago: Isotopic and trace-element constraints. *Geochimica et Cosmochimica Acta*, *52*(12), 2979–2992. https://doi.org/10.1016/0016-7037(88)90162-7

Grevemeyer, I. (2023). Multibeam bathymetry raw data (Atlas Hydrosweep DS 2 echo sounder entire dataset) of RV METEOR during cruise M62/3 [Dataset]. *PANGAEA*. https://doi.org/10.1594/PANGAEA.960035

Grevemeyer, I., Helffrich, G., Faria, B., Booth Rea, G., Schnabel, M., & Weinrebe, W. (2009). Seismic activity at Cadamosto seamount near Fogo Island, Cabo Verdes - Formation of a new ocean island? *Geophysical Journal International*, *180*(2), 552–558. https://doi.org/10.1111/j.1365-246X.2009.04440.x

Grunau, H. R., Lehner, P., Cleintuar, M. R., Allenbach, P., & Bakker, G. (1975). New radiometric ages and seismic data from Fuerteventura (Canary Islands), Maio (Cape Verde Islands), and Sao Tomé (Gulf of Guinea). In G. J. Borradaile (Ed.), *Progress in Geodynamics* (pp. 90–118). Koninklijke Nederlandse Akademie van Wetenshappen.

Gudmundsson, A., Drymoni, K., Browning, J., Acocella, V., Amelung, F., Bonali, F. L., et al. (2022). Volcanotectonics: The tectonics and physics of volcanoes and their eruption mechanics. *Bulletin of Volcanology*, *84*(72), 72. https://doi.org/10.1007/s00445-022-01582-4

Hansteen, T., Kwasnitschka, T., & Klügel, A. (2014). *Cape Verde Seamounts - cruise no. M80/3: December 29, 2009–February 1, 2010—Dakar (Senegal)—Las Palmas de Gran Canaria (Spain)* (pp. 1–42). DFG-Senatskommission für Ozeanographie. https://doi.org/10.2312/cr_m80_3

Hansteen, T. H., Kwasnitschka, T., & Wölfl, A.-C. (2021). Multibeam bathymetry raw data (EM 120 echosounder entire dataset) of RV METEOR during cruise M80/3 [Dataset]. *PANGAEA*. https://doi.org/10.1594/PANGAEA.935344

Heleno, S. I., Faria, B. V., Bandomo, Z., & Fonseca, J. F. (2006). Observations of high-frequency harmonic tremor in Fogo, Cabo Verde Islands. *Journal of Volcanology and Geothermal Research*, *158*(3–4), 361–379. https://doi.org/10.1016/j.jvolgeores.2006.06.018

Helffrich, G., Heleno, S. I., Faria, B., & Fonseca, J. F. (2006). Hydroacoustic detection of volcanic ocean-island earthquakes. *Geophysical Journal International*, *167*(3), 1529–1536. https://doi.org/10.1111/j.1365-246X.2006.03228.x

Hill, I. (1985). *Geophysical studies of the Cabo Verde Archipelago*. *RRS Charles Darwin Cruise Report 8-85*. University of Leicester.

Holm, P. M., Grandvuinet, T., Friis, J., Wilson, J. R., Barker, A. K., & Plesner, S. (2008). An ^{40}Ar-^{39}Ar study of the Cabo Verde hot spot: Temporal evolution in a semistationary plate environment. *Journal of Geophysical Research*, *113*(B8201), 1–22. https://doi.org/10.1029/2007JB005339

Holm, P. M., Wilson, J. R., Christensen, B. P., Hansen, L., Hansen, S. L., Hein, K. M., et al. (2006). Sampling the Cabo Verde mantle plume: Evolution of melt compositions on Santo Antao, Cabo Verde Islands. *Journal of Petrology*, *47*(1), 145–189. https://doi.org/10.1093/petrology/egi071

Jena, B., Kurian, P. J., Swain, D., Tyagi, A., & Ravindra, R. (2012). Prediction of bathymetry from satellite altimeter based gravity in the Arabian Sea: Mapping of two unnamed deep seamounts. *International Journal of Applied Earth Observation and Geoinformation*, *16*, 1–4. https://doi.org/10.1016/j.jag.2011.11.008

Johnson, M. E., Baarli, B. G., Cachão, M., Mayoral, E., Ramalho, R. S., Santos, A., & da Silva, C. M. (2018). On the rise and fall of oceanic islands: Towards a global theory following the pioneering studies of Charles Darwin and James Dwight Dana. *Earth-Science Reviews*, *180*, 17–36. https://doi.org/10.1016/j.earscirev.2018.03.008

Jørgensen, J. Ø., & Holm, P. M. (2002). Temporal variation and carbonatite contamination in primitive ocean island volcanics from Sao Vicente, Cabo Verde Islands. *Chemical Geology*, *192*(3), 249–267. https://doi.org/10.1016/S0009-2541(02)00198-5

Klügel, A., Walter, T. R., Schwarz, S., & Geldmacher, J. (2005). Gravitational spreading causes en-echelon diking along a rift zone of Madeira Archipelago: An experimental approach and implications for magma transport. *Bulletin of Volcanology*, *68*(1), 37–46. https://doi.org/10.1007/s00445-005-0418-6

Lancelot, Y., Seibold, E., Cepek, P., Dean, W., Eremeev, V., Gardner, J., et al. (1978). Site 368: Cabo Verde Rise. In Y. Lancelot, E. Seibold, & J. V. Gardner (Eds.), *Initial Report of the Deep Sea Drilling Project* (Vol. 41, pp. 223–326). U.S. Government Printing Office.

Le Bas, T. P., Masson, D. G., Holtom, R. T., & Grevemeyer, I. (2007). Slope failures of the flanks of the southern Cabo Verde Islands. In V. Lykousis, D. Sakellariou, & J. Locat (Eds.), *Submarine mass movements and their consequences* (pp. 337–345). Springer.

Leitão, F., Dias, G., Ramalho, R., & Kwasnitschka, T. (2024). Multibeam bathymetry processed data (Kongsberg EM710 & EM 120 echosounder dataset compilation) of NRP ALMIRANTE GAGO COUTINHO during cruise HI_09A/20 [Dataset]. *PANGAEA*. https://doi.org/10.1594/PANGAEA.965479

Leva, C., Rümpker, G., & Wölbern, I. (2020). Remote monitoring of seismic swarms and the August 2016 seismic crisis of Brava, Cabo Verde, using array methods. *Natural Hazards and Earth System Sciences*, *20*(12), 3627–3638. https://doi.org/10.5194/nhess-20-3627-2020

Leva, C., Rümpker, G., & Wölbern, I. (2022). Multi-array analysis of volcano-seismic signals at Fogo and Brava, Cape Verde. *Solid Earth*, *13*(8), 1243–1258. https://doi.org/10.5194/se-13-1243-2022

Lodge, A., & Helffrich, G. (2006). Depleted swell root beneath the Cabo Verde Islands. *Geology*, *34*(6), 449–452. https://doi.org/10.1130/G22030.1

Madeira, J., Mata, J., Mourão, C., Brum da Silveira, A., Martins, S., Ramalho, R., & Hoffmann, D. L. (2010). Volcano-stratigraphic and structural evolution of Brava Island (Cabo Verde) based on ^{40}Ar/^{39}Ar, U–Th and field constraints. *Journal of Volcanology and Geothermal Research*, *196*(3–4), 219–235. https://doi.org/10.1016/j.jvolgeores.2010.07.010

Madeira, J., Munhá, J., Tassinari, C., Mata, J., Brum da Silva, A., & Martins, S. (2005). K/Ar ages of carbonatites from the Island of Fogo (Cape Verde). In *Proceedings of the XIV semana de Geoquímica/VIII Congresso de Geoquímica dos Países de Língua Portuguesa Lisboa, Portugal* (pp. 475–478).

Marques, F. O., Hildenbrand, A., Zeyen, H., Cunha, C., & Victória, S. S. (2020). The complex vertical motion of intraplate oceanic islands assessed in Santiago Island, Cape Verde. *Geochemistry, Geophysics, Geosystems*, *21*(3), e2019GC008754. https://doi.org/10.1029/2019gc008754

Masson, D. G., Le Bas, T. P., Grevemeyer, I., & Weinrebe, W. (2008). Flank collapse and large-scale landsliding in the Cabo Verde Islands, off West Africa. *Geochemistry, Geophysics, Geosystems*, *9*(7), Q07015. https://doi.org/10.1029/2008GC001983

Mata, J., Martins, S., Mattielli, N., Madeira, J., Faria, B., Ramalho, R. S., et al. (2017). The 2014–15 eruption and the short-term geochemical evolution of the Fogo volcano (Cabo Verde): Evidence for small-scale mantle heterogeneity. *Lithos*, *288*, 91–107. https://doi.org/10.1016/j.lithos.2017.07.001

Mata, J., Moreira, M., Doucelance, R., Ader, M., & Silva, L. C. (2010). Noble gas and carbon isotopic signatures from Cabo Verde oceanic carbonatites: Implications for carbon provenance. *Earth and Planetary Science Letters*, *291*(1–4), 70–83. https://doi.org/10.1016/j.epsl.2009.12.052

McNutt, M. (1988). Thermal and mechanical properties of the Cabo Verde Rise. *Journal of Geophysical Research*, *93*(B4), 2784–2794. https://doi.org/10.1029/JB093iB04p02784

Merle, O., & Borgia, A. (1996). Scaled experiments of volcanic spreading. *Journal of Geophysical Research*, *101*(B6), 13805–13817. https://doi.org/10.1029/95JB03736

Miller, K. G., Mountain, G. S., Wright, J. D., & Browning, J. V. (2011). A 180-million-year record of sea level and ice volume variations from continental margin and deep-sea isotopic records. *Oceanography*, *24*(2), 40–53. https://doi.org/10.5670/oceanog.2011.26

Mitchell, J. G., Le Bas, M. J., Zielonka, J., & Furnes, H. (1983). On dating the magmatism of Maio, Cabo Verde islands. *Earth and Planetary Science Letters*, *64*(1), 61–76. https://doi.org/10.1016/0012-821X(83)90053-5

Mitchell, N. C. (2001). Transition from circular to stellate forms of submarine volcanoes. *Journal of Geophysical Research*, *106*(B2), 2156–2202. https://doi.org/10.1029/2000JB900263

Mitchell, N. C., Dade, W. B., & Masson, D. G. (2003). Erosion of the submarine flanks of the Canary Islands. *Journal of Geophysical Research*, *108*(F1), 6002. https://doi.org/10.1029/2002JF000003

Monteiro, P., Ribeiro, D., Silva, J. A., Bispo, J., & Gonçalves, J. M. S. (2008). Ichthyofauna assemblages from two unexplored Atlantic seamounts: Northwest Bank and João Valente Bank (Cabo Verde Archipelago). *Scientia Marina*, *72*(1), 133–143. https://doi.org/10.3989/scimar.2008.72n1133

Morgan, W. J. (1971). Convection plumes in the lower mantle. *Nature*, *230*(5288), 42–43. https://doi.org/10.1038/230042a0

Mourão, C., Mata, J., Doucelance, R., Madeira, J., Millet, M. A., & Moreira, M. (2012). Geochemical temporal evolution of Brava Island magmatism: Constraints on the variability of Cabo Verde mantle sources and on carbonatite-silicate magmas link. *Chemical Geology*, *334*, 44–61. https://doi.org/10.1016/j.chemgeo.2012.09.031

Müller, R. D., Sdrolias, M., Gaina, C., & Roest, W. R. (2008). Age, spreading rates, and spreading asymmetry of the world's ocean crust. *Geochemistry, Geophysics, Geosystems*, *9*(4), Q04006. https://doi.org/10.1029/2007GC001743

Pim, J., Peirce, C., Watts, A. B., Grevemeyer, I., & Krabbenhöft, A. (2008). Crustal structure and origin of the Cabo Verde Rise. *Earth and Planetary Science Letters*, *272*(1–2), 422–428. https://doi.org/10.1016/j.epsl.2008.05.012

Plesner, S., Holm, P. M., & Wilson, J. R. (2002). ^{40}Ar-^{39}Ar geochronology of Santo Antão, Cabo Verde Islands. *Journal of Volcanology and Geothermal Research*, *120*(1–2), 103–121. https://doi.org/10.1016/S0377-0273(02)00367-0

Pollitz, F. F. (1991). Two-stage model of African absolute motion during the last 30 million years. *Tectonophysics*, *194*(1), 91–106. https://doi.org/10.1016/0040-1951(91)90274-V

Ramalho, R. S. (2011). *Building the Cabo Verde Islands*. Springer. https://doi.org/10.1007/978-3-642-19103-9

Ramalho, R. S., Helffrich, G., Cosca, M., Vance, D., Hoffmann, D., & Schmidt, D. N. (2010a). Episodic swell growth inferred from variable uplift of the Cabo Verde hotspot islands. *Nature Geosciences*, *3*(11), 774–777. https://doi.org/10.1038/ngeo982

Ramalho, R. S., Helffrich, G., Cosca, M., Vance, D., Hoffmann, D., & Schmidt, D. N. (2010b). Vertical movements of ocean island volcanoes: Insights from a stationary plate environment. *Marine Geology*, *275*(1–4), 84–95. https://doi.org/10.1016/j.margeo.2010.04.009

Ramalho, R. S., Helffrich, G., Madeira, J., Cosca, M., Thomas, C., Quartau, R., et al. (2017). Emergence and evolution of Santa Maria Island (Azores) - The conundrum of uplifted islands revisited. *Geological Society of America Bulletin*, *129*(3–4), 372–390. https://doi.org/10.1130/B31538.1

Ramalho, R. S., Helffrich, G., Schmidt, D. N., & Vance, D. (2010). Tracers of uplift and subsidence in the Cabo Verde Archipelago. *Journal of the Geological Society*, *167*(3), 519–538. https://doi.org/10.1007/978-3-642-19103-9_5

Ramalho, R. S., Quartau, R., Trenhaile, A. S., Mitchell, N. C., Woodroffe, C. D., & Ávila, S. P. (2013). Coastal evolution on volcanic oceanic islands: A complex interplay between volcanism, erosion, sedimentation, sea-level change and biogenic production. *Earth-Science Reviews*, *127*, 140–170. https://doi.org/10.1016/j.earscirev.2013.10.007

Ribeiro, O. (1960). A ilha do Fogo e as suas erupções. *Junta de investigações do ultramar, Memórias Série Geográfica* (Vol. *1*).

Ryan, W. B. F., Carbotte, S. M., Coplan, J. O., O'Hara, S., Melkonian, A., Arko, R., et al. (2009). Global multi-resolution topography synthesis. *Geochemistry, Geophysics, Geosystems*, *10*(3), Q03014. https://doi.org/10.1029/2008GC002332

Samrock, L. K., Wartho, J. A., & Hansteen, T. H. (2019). ^{40}Ar-^{39}Ar geochronology of the active phonolitic Cadamosto Seamount, Cabo Verde. *Lithos*, *344–345*, 464–481. https://doi.org/10.1016/j.lithos.2019.07.003

Schmidt, R., & Schmincke, H.-U. (2000). Seamounts and island building. In H. Sigurdsson & B. F. Houghton (Eds.), *Encyclopedia of volcanoes* (pp. 383–402). Elsevier/Academic Press.

Sleep, N. H. (1990). Hotspots and mantle plumes: Some phenomenology. *Journal of Geophysical Research*, *95*(B5), 6715–6736. https://doi.org/10.1029/JB095iB05p06715

Smith, W. H., & Sandwell, D. T. (1997). Global sea floor topography from satellite altimetry and ship depth soundings. *Science*, *277*(5334), 1956–1962. https://doi.org/10.1126/science.277.5334.1956

Sohn, R. A., Willis, C., Humphris, S., Shank, T. M., Singh, H., Edmonds, H. N., et al. (2008). Explosive volcanism on the ultraslow-spreading Gakkel ridge, Arctic Ocean. *Nature*, *453*(7199), 1236–1238. https://doi.org/10.1038/nature07075

Steiger, R. H., & Jäger, E. (1977). Subcommission on geochronology: Convention on the use of decay constants in geo- and cosmochronology. *Earth and Planetary Science Letters*, *36*(3), 359–362. https://doi.org/10.1016/0012-821X(77)90060-7

Stillman, C. J., Furnes, H., Le Bas, M. J., Robertson, A. H. F., & Zielonka, J. (1982). The geological history of Maio, Cabo Verde islands. *Journal of the Geological Society*, *139*(3), 347–361. https://doi.org/10.1144/gsjgs.139.3.0347

Torres, P. C., Madeira, J., Silva, L. C., Brum da Silveira, A., Serralheiro, A., & Mota Gomes, A. (1997). Carta geológica das erupções históricas da Ilha do Fogo: Revisão e actualização. *Comunicacoes do Instituto Geologico e Mineiro*, *84*(1), A193–A196.

Torres, P. C., Silva, L. C., Serralheiro, A., & Tassinari, C. (2002). Geochronological framework with the K/Ar method of the main volcano-stratigraphic sequences of Sal Island - Cabo Verde. *Garcia de Orta*, *18*(1–2), 9–13.

Waelbroeck, C., Labeyrie, L., Michel, E., Duplessy, J. C., Mcmanus, J. F., Lambeck, K., et al. (2002). Sea-level and deep water temperature changes derived from benthic foraminifera isotopic records. *Quaternary Science Reviews*, *21*(1–3), 295–305. https://doi.org/10.1016/S0277-3791(01)00101-9

Walter, T., Klügel, A., & Münn, S. (2006). Gravitational spreading and formation of new rift zones on overlapping volcanoes. *Terra Nova*, *18*(1), 26–33. https://doi.org/10.1111/j.1365-3121.2005.00656.x

Wang, S., Yu, H., Zhang, Q., & Zhao, Y. (2018). Absolute plate motions relative to deep mantle plumes. *Earth and Planetary Science Letters*, *490*, 88–99. https://doi.org/10.1016/j.epsl.2018.03.021

Wartho, J., Samrock, L. K., & Kwasnitschka, T. (2024). ^{40}Ar-^{39}Ar data table of single-/multi-crystal laser total fusion biotite and K-feldspar from Senghor Seamount, Cabo Verde (Meteor cruise M79/3, sample 950-2) [Dataset]. *PANGAEA*. https://doi.org/10.1594/PANGAEA.964858

White, J. D. L., Smellie, J. L., & Clague, D. A. (2003). Introduction. In J. D. L. White, J. L. Smellie, & D. A. Clague (Eds.), *Explosive subaqueous volcanism*, *Geophysical Monograph Series* (pp. 1–24). American Geophysical Union.

Williams, C. A., Hill, I. A., Young, R., & White, R. S. (1990). Fracture zones across the Cabo Verde Rise, NE Atlantic. *Journal of the Geological Society*, *147*(5), 851–857. https://doi.org/10.1144/gsjgs.147.5.0851

Wilson, D. J., Peirce, C., Watts, A. B., & Grevemeyer, I. (2013). Uplift at lithospheric swells—II: Is the Cape Verde mid-plate swell supported by a lithosphere of varying mechanical strength? *Geophysical Journal International*, *193*(2), 798–819. https://doi.org/10.1093/gji/ggt034

Wilson, D. J., Peirce, C., Watts, A. B., Grevemeyer, I., & Krabbenhoeft, A. (2010). Uplift at lithospheric swells – I. Seismic and gravity constraints on the crust and uppermost mantle structure of the Cape Verde mid-plate swell. *Geophysical Journal International*, *182*(2), 531–550. https://doi.org/10.1111/j.1365-246X.2010.04641.x

References From the Supporting Information

Baksi, A. K. (2007). A quantitative tool for detecting alteration in undisturbed rocks and minerals—I: Water, chemical weathering, and atmospheric argon. In *Geological Society of America Special Paper 430: Plates, Plumes and Planetary Processes* (pp. 285–303). Geological Society of America. https://doi.org/10.1130/2007.2430(15)

Koppers, A. P. (2002). ArArCALC software for $^{40}Ar/^{39}Ar$ age calculations. *Computers and Geosciences*, *28*(5), 605–619. https://doi.org/10.1016/S0098-3004(01)00095-4

Renne, P. R., Deino, A. L., Hilgen, F. J., Kuiper, K. F., Mark, D. F., Mitchell, W. S., et al. (2013). Time scales of critical events around the Cretaceous-Paleogene boundary. *Science*, *339*(6120), 684–687. https://doi.org/10.1126/science.1230492

Renne, P. R., & Norman, E. B. (2001). Determination of the half-life of ^{37}Ar by mass spectrometry. *Physical Review C: Nuclear Physics*, *63*(4), 473021–473023. https://doi.org/10.1103/PhysRevC.63.047302

Renne, P. R., Sharp, Z. D., & Heizler, M. T. (2008). Cl-derived argon isotope production in the CLICIT facility of OSTR reactor and the effects of the Cl-correction in $^{40}Ar/^{39}Ar$ geochronology. *Chemical Geology*, *255*(3–4), 463–466. https://doi.org/10.1016/j.chemgeo.2008.07.014

Renne, P. R., Sprain, C. J., Richards, M. A., Self, S., Vanderkluysen, L., & Pande, K. (2015). State shift in Deccan volcanism at the Cretaceous-Paleogene boundary, possibly induced by impact. *Science*, *350*(6256), 76–78. https://doi.org/10.1126/science.aac7549

Stoenner, R. W., Schaeffer, O. A., & Katcoff, S. (1965). The half-lives of argon-37, argon-39, and argon-42. *Science*, *148*(3675), 1325–1328. https://doi.org/10.1126/science.148.3675.1325

van den Bogaard, P. (2013). The origin of the Canary Island Seamount Province—New ages of old seamounts. *Scientific Reports*, *3*(1), 2107. https://doi.org/10.1038/srep02107